

Theory of singular vortex solutions of the nonlinear Schrödinger equation

Gadi Fibich*, Nir Gavish

School of Mathematical Sciences, Tel Aviv University, Tel Aviv 69978, Israel

Received 8 November 2007; received in revised form 8 April 2008; accepted 15 April 2008
Available online 4 May 2008

Communicated by K. Promislow

Abstract

We present a systematic study of singular vortex solutions of the critical and supercritical two-dimensional nonlinear Schrödinger equation. In particular, we study the critical power for collapse and the asymptotic blowup profile of singular vortices.

© 2008 Elsevier B.V. All rights reserved.

PACS: 42.65.Jx; 42.65.-k

Keywords: Nonlinear Schrödinger equation; Vortex; Supercritical; Critical; Self-similar solution; Singularity; Collapse; Ring profile; Blowup rate; Critical power; Power concentration

1. Introduction

The focusing d -dimensional nonlinear Schrödinger equation (NLS)

$$i\psi_t(t, \mathbf{x}) + \Delta\psi + |\psi|^{2\sigma}\psi = 0, \quad \psi(0, \mathbf{x}) = \psi_0(\mathbf{x}), \quad (1)$$

where $\mathbf{x} = (x_1, x_2, \dots, x_d)$ and $\Delta = \partial_{x_1 x_1} + \dots + \partial_{x_d x_d}$, is one of the canonical nonlinear equations in physics, arising in various fields such as nonlinear optics, plasma physics, Bose–Einstein condensates (BEC), and surface waves. The NLS (1) is called *subcritical* if $\sigma d < 2$. In this case, all solutions exist globally. In contrast, solutions of the *critical* ($\sigma d = 2$) and *supercritical* ($\sigma d > 2$) NLS can become singular in finite time $0 < T_c < \infty$, i.e., $\lim_{t \rightarrow T_c} \|\psi\|_{H^1} = \infty$, where $\|\psi\|_{H^1} = \sqrt{\int |\psi|^2 dx + \int |\nabla\psi|^2 dx}$. See, e.g., [1] for more information.

In this study we consider singular solutions of the two-dimensional NLS, which in polar coordinates is given by

$$i\psi_t(t, r, \theta) + \psi_{rr} + \frac{1}{r}\psi_r + \frac{1}{r^2}\psi_{\theta\theta} + |\psi|^{2\sigma}\psi = 0, \quad \psi(0, r, \theta) = \psi_0(r, \theta). \quad (2)$$

This equation is critical when $\sigma = 1$ and supercritical when $\sigma > 1$. We focus on *vortex solutions* of the form

$$\psi(t, r, \theta) = A(t, r)e^{im\theta}, \quad m \in \mathbb{Z}. \quad (3)$$

It is relatively easy to produce optical vortices experimentally. As a result, vortices have been intensively studied, both theoretically and experimentally, in the nonlinear optics literature. More recently, vortex solutions have been studied, both theoretically and

* Corresponding author.

E-mail addresses: fibich@tau.ac.il (G. Fibich), nirgvsh@tau.ac.il (N. Gavish).

URL: <http://www.math.tau.ac.il/~fibich> (G. Fibich).

experimentally, in Bose–Einstein condensates (BEC).¹ However, almost all of this research effort has been on non-collapsing vortices. In fact, to the best of our knowledge, the only studies of collapsing vortex solutions are those of Kruglov and co-workers [3, 4] and of Vuong et al. [5]. Therefore, there is a huge gap between the available theory on non-vortex and vortex singular NLS solutions.

In this study, we present a systematic study of singular vortex solutions of the critical and supercritical NLS (2). In particular, we ask to what extent the available theory for singular NLS solutions remains valid for the subset of singular vortex solutions. Of course, all the rigorous results that were previously derived for singular NLS solutions remain valid for the special case of vortex solutions. As we shall see, however, in some cases stronger results can be obtained for collapsing vortices (e.g., the critical power for collapse). In addition, we find that some of the non-rigorous results for singular non-vortex solutions that were derived using asymptotic analysis and numerical simulations (e.g., stability of blowup profiles) do change for vortex solutions. Intuitively, the main reason for this qualitative difference is that vortex solutions must vanish at the origin, where the phase is undefined. Therefore, singular vortex solutions that collapse at the origin are identically zero there and must have a ring profile. This is very different from non-vortex singular solutions, whose amplitude at the collapse point increases to infinity as they collapse, regardless of whether their peak value is at the collapse point (i.e., peak-type solution) or not (i.e., ring-type solution).

The paper is organized as follows. In Section 2, we recall the conservation laws of the NLS (2). In Section 3, we consider stationary vortex solutions of the form $\psi_{m,k}^{\text{stationary}} = R_{m,k}(r)e^{i\lambda t + im\theta}$.

In Section 4, we systematically study vortex solutions of the *critical* ($\sigma = 1$) two-dimensional NLS

$$i\psi_t(t, r, \theta) + \psi_{rr} + \frac{1}{r}\psi_r + \frac{1}{r^2}\psi_{\theta\theta} + |\psi|^2\psi = 0, \quad \psi(0, r, \theta) = \psi_0(r, \theta). \quad (4)$$

In Section 4.1, we study the profiles $R_{m,k}(r)$ of the stationary vortex solutions and in particular the ground state profile $R_{m,0}$. In Section 4.2 we show that as in the vortex-free case, there are two types of explicit blowup solutions of the critical NLS (4): $\psi_{R_m}^{\text{explicit}}$ with a linear blowup rate which are in H^1 , and $\psi_{G_m}^{\text{explicit}}$ with a square-root blowup rate which are not in H^1 . However, while in the vortex-free case, $\psi_{R_0}^{\text{explicit}}$ is a peak-type solution and $\psi_{G_0}^{\text{explicit}}$ is a ring-type solution, in the vortex case, both $\psi_{R_m}^{\text{explicit}}$ and $\psi_{G_m}^{\text{explicit}}$ are ring-type solutions. Moreover, unlike $\psi_{G_0}^{\text{explicit}}$, these *singular vortex ring solutions are identically zero at the singularity point* $r = 0$. In Section 4.3 we consider the critical power (L^2 norm) for collapse in the critical NLS (4). Recall that in the non-vortex case the critical power is equal to $P_{\text{cr}} = \int |R_{0,0}|^2 r dr$, where $R_{0,0}$ is the ground state solution of

$$R'' + \frac{1}{r}R' - R + R^3 = 0, \quad R'(0) = 0, \quad R(\infty) = 0. \quad (5)$$

In contrast, the critical power for radially-symmetric vortex initial conditions of the form $\psi_0 = A_0(r)e^{im\theta}$ is $P_{\text{cr}}(m) = \int |R_{m,0}|^2 r dr$, where $R_{m,0}$ is the ground state solution of

$$R_m''(r) + \frac{1}{r}R_m' - \left(1 + \frac{m^2}{r^2}\right)R_m + R_m^3 = 0, \quad R_m'(0) = 0, \quad R_m(\infty) = 0.$$

The critical power $P_{\text{cr}}(m)$ increases with m , and is approximately given by $P_{\text{cr}}(m) \approx 4\sqrt{3}m$. In particular, it is significantly larger than $P_{\text{cr}} := P_{\text{cr}}(m = 0) \approx 1.86$. In [3], Kruglov and Logvin estimated the value of $P_{\text{cr}}(m)$ by assuming that the vortex solution collapses with a self-similar Laguerre-Gaussian profile. We show that this estimate is a crude upper bound, and that this is due to the use of the aberrationless approximation and the fact that the Laguerre-Gaussian profile does not provide a good approximation of $R_{m,0}$. In addition, we provide a simple criterion to determine whether an initial profile is “close” to $R_{m,0}$, in which case the excess power above $P_{\text{cr}}(m)$ needed for collapse is “small”. We then ask what is the critical power when the initial vortex profile is not radially-symmetric, e.g. when $\psi_0 = A_0(x, y)e^{im\theta}$ where A_0 is real but not symmetric in r . In Section 4.3.3 we show that in this case, the vortex solution can collapse with power *below* $P_{\text{cr}}(m)$ but, of course, above P_{cr} . This is exactly opposite from the non-vortex case, in which deviations from radial symmetry increase the threshold power for collapse [6]. The reason for this difference is as follows. In the vortex-free case, the $\psi_{R_{0,0}}$ profile is stable under symmetry-breaking perturbations. In contrast, vortices are unstable under symmetry-breaking perturbations and, when perturbed azimuthally, they break into a ring of filaments. Since these filaments do not collapse at $r = 0$, the vorticity does not prohibit them from collapsing with the $R_{0,0}$ profile. Hence, the critical power for collapse of each of the filaments is $P_{\text{cr}} = P_{\text{cr}}(m = 0)$. In Section 4.4 we show that as in the vortex-free case, all stationary vortex solutions are strongly unstable. In Section 4.5 we show that as in the vortex-free case, the explicit vortex blowup solution $\psi_{R_{m,0}}^{\text{explicit}}$ is unstable.

Section 4.6 is devoted to the study of the asymptotic blowup profiles of critical vortex solutions. In [7], Merle and Raphael proved that all singular solutions of the critical NLS (4) with power slightly above P_{cr} collapse with the asymptotic $\psi_{R_{0,0}}$ profile and that

¹ For a recent review on vortices in Optics and in BEC, see [2].

their blowup rate is a square root with a loglog correction (the *loglog law*). Although this result was proved only for solutions with power moderately above P_{cr} , it was believed that “all” stable singular solutions of the critical NLS collapse with the $\psi_{R_{0,0}}$ profile at a square-root blowup rate with a loglog correction. In 2005, we discovered singular solutions of the critical NLS that collapse with a different self-similar profile denoted by $\psi_{G_{0,0}}$ at a square-root blowup rate [8]. Since $R_{0,0}$ attains its maximum at $r = 0$, whereas $G_{0,0}$ attains its maximum at $r_{max} > 0$, we refer to $\psi_{R_{0,0}}$ and $\psi_{G_{0,0}}$ as self-similar ‘peak-type’ and ‘ring-type’ solutions, respectively. At present, it is still an open question whether the self-similar ring profile $\psi_{G_{0,0}}$ is maintained all the way up to the singularity or whether ultimately it changes into a peak-type $\psi_{R_{0,0}}$ profile.

In Section 4.6.1 we prove that all singular vortex solutions collapse with a self-similar profile. We then prove a concentration theorem for vortex solutions, namely that the amount of power that collapses into the singularity is at least the critical power $P_{cr}(m)$. This proves that radially-symmetric singular vortex solutions cannot collapse with the $\psi_{R_{0,0}}$ profile. We then ask what the asymptotic profile of singular vortex solutions is. A priori, there are two possible asymptotic profiles: $\psi_{R_{m,0}}$ with the loglog law blowup rate, and $\psi_{G_{m,0}}$ with a square-root blowup rate (Section 4.6.2). In Section 4.6.3, we conduct a numerical study to determine which of these two asymptotic profiles is stable. Our simulations suggest that radially-symmetric singular vortex solutions, i.e., solutions of the form (3), always collapse with a self-similar $\psi_{G_{m,0}}$ profile at a square-root blowup rate. In particular, even a perturbed $\psi_{R_{m,0}}$ vortex profile is observed to collapse with a self-similar $G_{m,0}$ profile at a square-root blowup rate. This result is surprising, since in the vortex-free case the profile $\psi_{R_{0,0}}$ is a strong attractor, and therefore a perturbed $\psi_{R_{0,0}}$ profile collapses with a self-similar $\psi_{R_{0,0}}$ profile at a faster-than-a-square-root blowup rate.

As noted, our simulations suggest that “all” radially-symmetric H^1 singular vortex solution of the critical NLS collapse with the $\psi_{G_{m,0}}$ profile at a square-root blowup rate. The $\psi_{G_{m,0}}$ profile, however, has an infinite power (L^2 norm). This seems to suggest that $\psi_{G_{m,0}}$ cannot be the asymptotic profile of H^1 vortex solutions of the critical NLS. However, in Section 4.6.4, we show that the collapsing solution is only *quasi-self-similar*, i.e., the self-similar profile $\psi_{G_{m,0}}$ characterizes only the collapsing ring region and not the whole solution. Therefore, the infinite-power tail of the vortex profile $G_{m,0}$ may be “irrelevant” to the NLS ring solutions. We recall that a similar situation appears in the vortex-free case $m = 0$, where $\psi_{G_{0,0}}$ characterizes only the collapsing ring region and not the whole solution so that the infinite-power tail of ψ_G is also “irrelevant” [8]. The numerical simulations in [8] show that H^1 ring solutions of the NLS collapse with an asymptotic quasi-self-similar blowup profile $\psi_{G_{0,0}}$ up to focusing levels of 10^{16} . However, it is impossible to determine numerically whether these solutions maintain a ring profile all the way until the singularity or whether at some exceedingly large focusing factor the ring structure breaks up and they collapse with the $\psi_{R_{0,0}}$ profile. It is therefore an open question whether there exist H^1 non-vortex solutions of the NLS that collapse with the self-similar ring profile $\psi_{G_{0,0}}$ at a square-root rate. *The surprising observation that the finite-power vortex solutions which start close to $\psi_{R_{m,0}}$ collapse as $\psi_{G_{m,0}}$ suggests that $\psi_{G_{m,0}}$ may, indeed, be the asymptotic quasi-self-similar profile of H^1 vortex solutions of the critical NLS all the way up to the singularity.* However, as in the vortex-free case, at present, whether this is indeed the case is an open question.

As noted, in Section 4.6.3 we observed numerically that the self-similar collapsing $\psi_{G_{m,0}}$ profile is stable with respect to radially-symmetric perturbations of the form $g(r)e^{im\theta}$. In Section 4.6.6, we ask if the collapsing $\psi_{G_{m,0}}$ profile is also stable in the general case, i.e., under asymmetric (azimuthal) perturbations. To answer this question analytically we use the azimuthal instability method [9,10] developed by Soto-Crespo and co-workers. This, however, requires some modifications to the method, since this method has only been derived for and applied to stationary vortex solutions. We show that collapsing vortices are unstable with respect to symmetry-breaking perturbations and that they break into a ring of filaments. Moreover, our analysis leads to a prediction of the number of filaments, which is in good agreement with our simulations.

The above results give rise to the following interesting scenario. Let us consider a slightly perturbed $\psi_{R_{m,0}}$ initial condition. If the initial deviation from radial-symmetry is sufficiently small, then initially the solution would approach the self-similar ring profile $\psi_{G_{m,0}}$ while collapsing. Subsequently, due to the azimuthal instability of $\psi_{G_{m,0}}$, the solution would break into a ring of filaments, each of which would collapse with the non-vortex $\psi_{R_{0,0}}$ profile.

In Section 5, we study singular vortex solutions of the *supercritical* NLS. Recall that there are two known stable asymptotic profiles of non-vortex singular solutions of the supercritical NLS: The self-similar peak-type profile ψ_{S_0} which collapses at a square-root blowup rate, and the self-similar ring-type profile ψ_Q , recently discovered in [11], which collapses at a $\sigma/2$ blowup rate. In Section 5.2, we show that there are two possible asymptotic profiles for non-vortex solutions of the supercritical NLS: $\psi_{S_{m,0}}$ which collapses at a square-root blowup rate, and ψ_{Q_m} which collapses at a $\sigma/2$ blowup rate.² In Section 5.3, we conduct a numerical study in order to determine which of these two asymptotic profiles is stable. Our simulations suggest that ψ_{Q_m} is a strong attractor for radially-symmetric vortex solutions of the supercritical NLS, while $\psi_{S_{m,0}}$ is unstable. Note that this is the same as in the critical NLS, where ψ_{G_m} , the vortex analog of the ring-type solution, is stable, while ψ_{R_m} , the vortex analog of the peak-type solution, is unstable.

In Section 6 we describe the numerical methods used in this study. Generally, the methods used for vortex simulations are the same methods used for non-vortex ring solutions in [8]. However, the simulations in the vortex case are more demanding than

² In [12], Budd et al. found ring (multi-bump) solutions of the supercritical NLS which are different from ψ_{Q_m} and $\psi_{S_{m,0}}$. These solutions, however, turned out to be unstable.

in the vortex-free case. The reason is that vortex solutions vanish at the origin, hence as they collapse the amplitude difference between the origin and the ring peak becomes larger and larger, contributing to huge gradients in the solution. In contrast, the value of non-vortex rings at the origin increases at the same rate as the maximal ring amplitude increases as it collapses. Hence, the amplitude difference between the origin and the ring peak remains constant during the collapse and is typically “only” two orders of magnitude.

The most surprising observation of this study is that the critical $\psi_{R_{m,0}}$ profile and the supercritical $\psi_{S_{m,0}}$ profile are unstable and therefore “all” critical vortices collapse with the $\psi_{G_{m,0}}$ profile at a square-root blowup rate and “all” supercritical vortices collapse with the ψ_{Q_m} profile at a $\sigma/2$ blowup rate. These observations are surprising, since in the vortex-free case $\psi_{R_{0,0}}$ and $\psi_{S_{0,0}}$ are stable asymptotic blowup profiles and in some sense are even “more stable” than $\psi_{G_{0,0}}$ and $\psi_{Q_{0,0}}$ since they are also stable under symmetry-breaking perturbations. This observation may also be relevant to the open question of whether there exist H^1 non-vortex ($m = 0$) or vortex solutions of the NLS that collapse with the self-similar ring profile $\psi_{G_{m,0}}$. Indeed, this problem might be easier to analyze in the vortex case, since $\psi_{G_{m,0}}$ seems to be the *only* possible asymptotic blowup profile of finite-power vortex solutions. In addition, this open problem may be easier to analyze in the vortex case from a technical point of view, since the $\psi_{G_{m,0}}$ vortex profile is self-similar not only in the ring region (as in the case of $\psi_{G_{0,0}}$) but also around the origin (Section 4.6.4). Therefore, the solution of this problem in the vortex case may provide the key to the solution in the non-vortex case.

2. Conservation laws

The two-dimensional NLS (2) has the following conservation laws:

- (1) Power (mass/ L^2 norm) conservation: $P(t) \equiv P(0)$, where

$$P(t) = \|\psi\|_2^2.$$

- (2) Hamiltonian conservation: $H(t) \equiv H(0)$, where

$$H(t) = \|\nabla\psi\|_2^2 - \frac{1}{\sigma + 1} \|\psi\|_{2\sigma+2}^{2\sigma+2}.$$

- (3) Angular momentum conservation: $M(t) \equiv M(0)$, where

$$M(t) = \int \mathbf{x} \times \text{Im}(\psi \nabla \psi^*) \, d\mathbf{x}.$$

We also recall that solutions of the NLS (2) satisfy the *Variance identity* [13]

$$V_{tt} = 8 \left[H(t) - \frac{\sigma - 1}{\sigma + 1} \|\psi\|_{2\sigma+2}^{2\sigma+2} \right],$$

where $V(t) = \|x\psi\|_2^2$ and $H(t)$ is the Hamiltonian of ψ . In the critical case $\sigma = 1$, the variance identity reduces to

$$V_{tt} = 8H. \tag{6}$$

Let us consider a vortex initial condition with winding number (topological charge) m , i.e.,

$$\psi_0(r, \theta) = A_0(r)e^{im\theta}, \quad m \in \mathbb{Z}. \tag{7}$$

In this case, the solution remains a vortex with winding number m :

Lemma 1. *Let ψ be a solution of the NLS (2) with the initial condition (7). Then,*

$$\psi(t, r, \theta) = A(t, r)e^{im\theta}, \tag{8}$$

where $A(t, r)$ is the solution of

$$iA_t(t, r) + A_{rr} + \frac{1}{r}A_r - \frac{m^2}{r^2}A + |A|^{2\sigma}A = 0, \quad A(0, r) = A_0(r). \tag{9}$$

Proof. Substituting $\psi = A(t, r)e^{im\theta}$ into the NLS gives that A is a solution of (9). Since θ does not appear in (9), A is independent of θ . Since $\psi = A(t, r)e^{im\theta}$ is a solution of the NLS, it follows from the uniqueness of NLS solution that (8) is the unique solution. \square

In light of Lemma 1, the NLS with the vortex initial condition (7) is equivalent to Eq. (9). The stability of these vortex solutions of the NLS (2) under perturbations of the initial condition which do not preserve the form (7) will be discussed in Section 4.6.6.

Lemma 2. Let ψ be a solution of the NLS (2) with a vortex initial condition $\psi_0 = A_0(r)e^{im\theta}$. Then,

- (1) $P(\psi) = P(A)$.
- (2) $\|\nabla\psi\|_2^2 = \|\frac{d}{dr}A\|_2^2 + m^2 \|\frac{A}{r}\|_2^2$.
- (3) $\|\psi\|_{H^1}^2 = \|A\|_2^2 + \|\frac{d}{dr}A\|_2^2 + m^2 \|\frac{A}{r}\|_2^2$.
- (4) $H(\psi) = H(A) + m^2 \|\frac{A}{r}\|_2^2$.
- (5) If $\psi(t, \cdot) \in H^1$, then $A(t, \cdot) \in \mathcal{F}$ where

$$\mathcal{F} = \left\{ f : \mathbb{R}^+ \rightarrow \mathbb{C} \mid f \neq 0, f, \frac{f}{r}, f_r \in L_2 \right\}. \tag{10}$$

- (6) $M(\psi) = mP(A)$.

Proof. See Appendix A. \square

3. Stationary vortex solutions ($\psi_{m,k}^{\text{stationary}}$)

We can look for a stationary vortex solution of the NLS (2) of the form $\psi_m^\lambda = R_m^\lambda(r)e^{i\lambda t + im\theta}$. Here $\frac{d\theta}{dt} = \frac{\lambda}{m}$ is the rotation speed, and $R_m^\lambda(r)$ is the solution of

$$(R_m^\lambda)''(r) + \frac{1}{r}(R_m^\lambda)' - \left(\lambda + \frac{m^2}{r^2} \right) R_m^\lambda + (R_m^\lambda)^{2\sigma+1} = 0, \quad (R_m^\lambda)'(0) = 0, \quad R_m^\lambda(\infty) = 0. \tag{11}$$

Let us define

$$R_m^\lambda = \lambda^{\frac{1}{2\sigma}} R_m(\sqrt{\lambda}r). \tag{12}$$

Then, R_m is the solution of

$$R_m''(r) + \frac{1}{r}R_m' - \left(1 + \frac{m^2}{r^2} \right) R_m + R_m^{2\sigma+1} = 0, \quad R_m'(0) = 0, \quad R_m(\infty) = 0. \tag{13}$$

Therefore, up to scaling, the vortex profile R_m^λ is independent of λ . Hence, without loss of generality, we can assume that $\lambda = 1$ and $m > 0$. In this case,

$$\psi_m^{\text{stationary}} = R_m(r)e^{it + im\theta} \tag{14}$$

rotates anti-clockwise at a speed of $1/m$.

We now consider the behavior of $R_m(r)$ near $r = 0$:

Lemma 3. Let $R_m(r)$ be a solution of (13). Then $R_m(r) = r^m q_m(r)$, where $q_m(0) \neq 0$ and $q_m(r)$ is the analytic solution of

$$q_m''(r) + \frac{2m+1}{r}q_m' - q_m + r^{2\sigma m}q_m^{2\sigma+1} = 0, \quad q_m'(0) = 0, \quad q_m(\infty) = 0. \tag{15}$$

Proof. See Appendix B. \square

The following results are known:

- (1) For any integer m , any $\sigma > 0$, and any $k = 0, 1, \dots$, there exists a solution $R_{m,k}(r)$ of (13) in H^1 that has exactly k nodes in $(0, \infty)$ [14].
- (2) Uniqueness for $k = 0$: For any integer m and for any $\sigma > 0$, there exists a unique solution $R_{m,k=0}$ of (13) in H^1 which is positive in $(0, \infty)$ [15]. Uniqueness for $k \geq 1$ is open.
- (3) For any integer m , any $\sigma > 1$ (i.e., the supercritical NLS), and any $k = 0, 1, \dots$, the stationary vortex solution (14) is linearly unstable under perturbations of the initial condition of the form $g(r)e^{im\theta}$ [15,16].
- (4) The positive vortex solution $R_{m,0} := R_{m,k=0}$ of (13) can be approximated as follows [17]:

Lemma 4.

$$R_{m,0}(r) \approx \left(1 + \frac{m^2}{r_{\max}^2} \right)^{\frac{1}{2\sigma}} (1 + \sigma)^{\frac{1}{2\sigma}} \operatorname{sech}^{\frac{1}{\sigma}} \left(\sqrt{1 + \frac{m^2}{r_{\max}^2}} \sigma (r - r_{\max}) \right), \quad m \gg 1, \tag{16a}$$

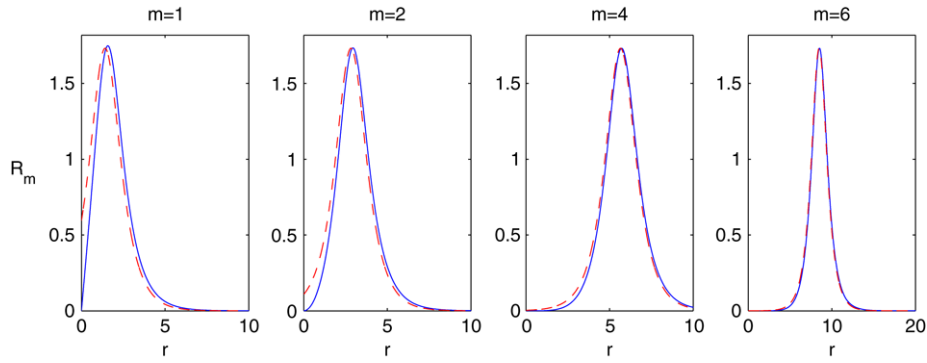


Fig. 1. The ground state profile $R_{m,0}(r)$ of Eq. (18) for $m = 1, 2, 4,$ and 6 (solid). The dashed curve is the approximation (19).

where

$$r_{\max} \approx \sqrt{\frac{2}{\sigma}} m. \tag{16b}$$

This result is proved in [17, Lemma 3] by expansion in $m \gg 1$.

In addition, the following scaling laws have been found numerically [18] for $k \rightarrow \infty$,

$$q_{m,k}(0) \sim k^{\frac{1+m\sigma}{2}}, \quad \|R_{m,k}\|_2 \sim k, \quad \|\nabla R_{m,k}\|_2 \sim k.$$

4. Critical case ($\sigma = 1$)

We now consider vortex solutions $\psi = A(t, r)e^{im\theta}$ of the two-dimensional critical NLS (4). In this case, Eq. (9) for $A(t, r)$ becomes

$$iA_t(t, r) + A_{rr} + \frac{1}{r}A_r - \frac{m^2}{r^2}A + |A|^2A = 0, \quad A(0, r) = A_0(r). \tag{17}$$

4.1. Ground state vortex profile ($R_{m,0}$)

In the critical case, Eq. (13) becomes

$$R_m''(r) + \frac{1}{r}R_m'(r) - \left(1 + \frac{m^2}{r^2}\right)R_m + R_m^3 = 0, \quad R_m'(0) = 0, \quad R_m(\infty) = 0. \tag{18}$$

As noted, this equation has an enumerable number of solutions $\{R_{m,k}\}_{k=0}^\infty$ in \mathcal{F} .

Definition 5. The ground state of (18) is the minimal power solution of Eq. (18) in \mathcal{F} .

Lemma 6. The ground state of (18) is given by $R_{m,0}$.

Proof. See Appendix C. \square

By Lemma 4, the profile of the ground state of (18) can be approximated as

$$R_{m,0}(r) \approx \sqrt{3} \operatorname{sech}\left(\frac{r - r_{\max}}{\sqrt{2/3}}\right), \quad m \gg 1, \tag{19}$$

where $r_{\max} \approx \sqrt{2}m$.

A comparison between $R_{m,0}$ and the approximation (19) is given in Fig. 1. As expected, since the approximation (19) was derived by expansion in $m \gg 1$, it becomes more accurate as m increases.

For later reference (see Section 4.3.1), we note that for $R_{m,0}^\lambda(r) = \sqrt{\lambda}R_{m,0}(\sqrt{\lambda}r)$, see Eq. (12),

$$R_{m,0}^\lambda(r) \approx \ell^\lambda \operatorname{sech}\left(\frac{r - r_{m,0}^\lambda}{L^\lambda}\right), \quad m \gg 1, \tag{20}$$

where $\ell^\lambda \approx \sqrt{3\lambda}$, $L^\lambda \approx \sqrt{\frac{2}{3\lambda}}$, $r_{m,0}^\lambda \approx \frac{\sqrt{2}m}{\sqrt{\lambda}}$.

4.2. Explicit blowup solutions

Recall that in the case $m = 0$ there are two types of explicit blowup solutions [8]:

- (1) A peak-type solution ψ_R^{explicit} with a linear blowup rate, which is in H^1 .
- (2) A ring-type solution ψ_G^{explicit} with a square-root blowup rate, which is not in H^1 .

We now show that this is also the case for $m > 0$, namely, there are two types of explicit blowup solutions:

- (1) $\psi_{R_m}^{\text{explicit}}$ with a linear blowup rate, which is in H^1 .
- (2) $\psi_{G_m}^{\text{explicit}}$ with a square-root blowup rate, which is not in H^1 .

Unlike the vortex-free case, however, both solutions are ring-type.

4.2.1. Linear blowup rate ($\psi_{R_m}^{\text{explicit}}$)

The critical NLS (4) is invariant under the following lens (pseudo-conformal) transformation [19]. Let ψ be a solution of the critical NLS (4), let

$$\tilde{\psi}(t, r, \theta) = \frac{1}{L(t)} \psi(\tau, \rho, \theta) \exp\left(i \frac{L_t}{L} \frac{r^2}{4}\right), \tag{21a}$$

where

$$\rho = \frac{r}{L(t)}, \quad \tau = \int_0^t \frac{ds}{L^2(s)}, \tag{21b}$$

and $L(t) = f_c(T_c - t)$. Then, $\tilde{\psi}$ is also a solution of the NLS (4).

Applying the lens transformation (21) to the stationary vortex solutions $\psi_{m,k}^{\text{stationary}} = R_{m,k}(r)e^{it+im\theta}$ gives rise to the explicit vortex blowup solutions

$$\psi_{R_{m,k}}^{\text{explicit}}(t, r, \theta) = \frac{1}{L(t)} R_{m,k}\left(\frac{r}{L(t)}\right) e^{i \int_0^t \frac{ds}{L^2(s)} + im\theta + i \frac{L_t}{L} \frac{r^2}{4}}, \quad L(t) = f_c(T_c - t), \tag{22}$$

where $f_c > 0$, and $R_{m,k}$ is a nontrivial solution of (18). Clearly, $\psi_{R_{m,k}}^{\text{explicit}}$ blow up at $r = 0$ as $t \rightarrow T_c$, since for all $\varepsilon > 0$,

$$\lim_{t \rightarrow T_c} \int_{r < \varepsilon} |\nabla \psi_{R_{m,k}}^{\text{explicit}}|^2 r dr d\theta = \infty. \tag{23}$$

Since $R_{m,k}(0) = 0$, see Lemma 3, it follows that $\psi_{R_{m,k}}^{\text{explicit}}(t, r = 0, \theta) \equiv 0$. Hence, $\psi_{R_{m,k}}^{\text{explicit}}$ are singular solutions that vanish at the singularity point $r = 0$. This is different from all non-vortex singular NLS solutions, e.g., the R profile and the G profile solutions, which become infinite at the singularity point [8,1].

The blowup rate of the explicit blowup solutions is linear, since

$$\|\nabla \psi_{R_{m,k}}^{\text{explicit}}\|_2^{-1} \sim c(T_c - t), \quad t \rightarrow T_c,$$

where $c = f_c / \|\nabla R_{m,k}\|_2$.

The phase of the explicit blowup solutions at a given rescaled radius $\rho = r/L(t)$ is

$$\theta(t) = -\frac{1}{m} \int_0^t \frac{ds}{L^2(s)} - \frac{L L_t}{4m} \rho^2 = \theta(0, \rho) - \frac{f_c^2}{4m} \rho^2 t - \tilde{\theta}(t), \tag{24}$$

where

$$\theta(0, \rho) = \frac{f_c^2}{4m} \rho^2 T_c, \quad \tilde{\theta}(t) = \frac{1}{m} \int_0^t \frac{1}{L^2} = \frac{1}{m f_c^2} \frac{1}{T_c - t}.$$

The phase is composed of the two radially-dependent terms $\theta(0, \rho) - \frac{f_c^2}{4m} \rho^2 t$, and the uniform phase term $-\tilde{\theta}(t)$. The second phase term $-\frac{f_c^2}{4m} \rho^2 t$ increases linearly in time and distorts the phase of the vortex into a spiral form, see Fig. 2. As $t \rightarrow T_c$,

$$\theta(t, \rho) \sim \theta(0, \rho) - \frac{f_c^2}{4m} \rho^2 T_c - \tilde{\theta}(t), \quad \tilde{\theta}(t) \rightarrow \infty. \tag{25}$$

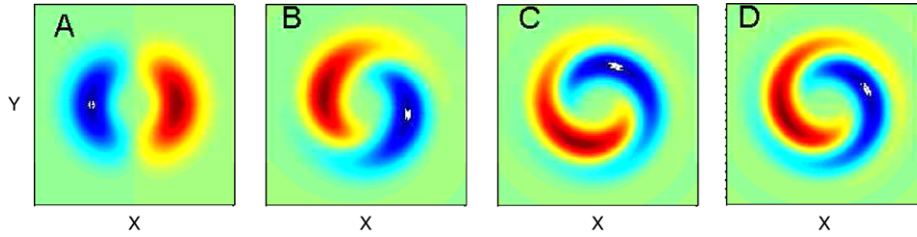


Fig. 2. $\text{Im} \left[R_{m=1, k=0}(\rho) e^{i\theta + i\tau - \frac{f_c^2}{4} \rho^2 t} \right]$ with $f_c = 0.75$ and $T_c = 5$ at A: $1/L = 1$ ($t = 0$), B: $1/L = 2$ ($t = 2.5$), C: $1/L = 10$ ($t = 4.5$), D: $1/L = 100$ ($t = 4.95$).

Therefore, near the singularity (i.e., for $t \sim T_c$) the radial phase distortion “freezes” and the phase simply rotates uniformly at the rotation speed $\frac{d}{dt} \tilde{\theta}(t) = -\frac{1}{m} \frac{1}{L^2}$, which increases to infinity as the vortex collapses,³ see Fig. 2(C) and (D).

4.2.2. Square-root blowup rate ($\psi_{G_m}^{\text{explicit}}$)

Let us consider explicit blowup solutions of the critical NLS (4) of the form

$$\psi(t, r, \theta) = \psi_{A_m}(t, r, \theta),$$

where

$$\psi_{A_m}(t, r) = \frac{1}{L(t)} A_m(\rho) e^{i\tau + im\theta + iLL_t \frac{\rho^2}{4}}, \quad \tau = \int_0^t \frac{ds}{L^2(s)}, \quad \rho = \frac{r}{L(t)}. \tag{26}$$

Note that ψ_{A_m} is of the form (22), except that we do not necessarily assume a linear blowup rate.

Substitution of ψ_{A_m} into the critical NLS (4) gives the following equation for A_m

$$A_m''(\rho) + \frac{1}{\rho} A_m' - \left(1 + \frac{m^2}{\rho^2} \right) A_m - \frac{1}{4} \beta(t) \rho^2 A_m + A_m^3 = 0, \quad \beta(t) = L^3 L_{tt}. \tag{27}$$

Since $A_m(\rho)$ is independent of t , $\beta(t) \equiv \beta_0$. Hence, the equation for $L(t)$ is

$$L_{tt} = -\beta_0 / L^3. \tag{28}$$

If $\beta_0 = 0$, then Eq. (27) for A_m becomes Eq. (18) for R_m , and L is linear in t , i.e., $A_m = R_m$ and we recover the blowup solutions $\psi_{R_m}^{\text{explicit}}$. If $\beta_0 > 0$, then by multiplying (28) by L_t and integrating we obtain that $(LL_t)^2 = \beta_0 + C_0 L^2$. Since $\lim_{t \rightarrow T_c} L(t) = 0$,

$$\lim_{t \rightarrow T_c} (LL_t)^2 = \beta_0.$$

Hence, the blowup rate is a *square root*, i.e., $L(t) \sim f_c \sqrt{T_c - t}$, where $f_c^2 = 2\sqrt{\beta_0}$. In this case, we denote $A_m = G_m$, and the equation for G_m is

$$G_m''(\rho) + \frac{1}{\rho} G_m' - \left(1 + \frac{m^2}{\rho^2} - \frac{f_c^4}{16} \rho^2 \right) G_m + G_m^3 = 0. \tag{29}$$

Therefore,

$$\psi_{G_m}^{\text{explicit}}(t, r) = \frac{1}{L(t)} G_m(\rho) e^{i\tau + im\theta - i \frac{f_c^2}{8} \rho^2}, \tag{30a}$$

where

$$L(t) = f_c \sqrt{T_c - t}, \quad \tau = \int_0^t \frac{ds}{L^2(s)}, \quad \rho = \frac{r}{L(t)}, \tag{30b}$$

and G_m is the solution of (29), is an explicit blowup solution that has a square-root blowup rate.

³ The acceleration of the uniform rotation speed follows from the conservation of angular momentum. Indeed, as the power (mass) of the vortex contracts into a smaller region, the rotation speed must become faster in order to conserve angular momentum.

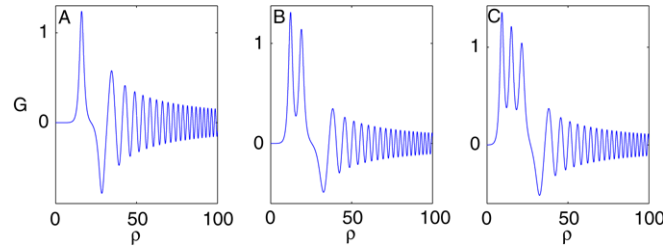


Fig. 3. Solutions of (29) with $m = 2$ and $f_c = 0.35$ for various values of g_0 : A: $g_0 = 6.5 \times 10^{-7}$. B: $g_0 = 2 \times 10^{-5}$. C: $g_0 = 3.5 \times 10^{-4}$.

Lemma 7. Let $G_m(r)$ be a solution of (29). Then $G_m(r) = r^m g_m(r)$, where $g_0 = g_m(0) \neq 0$ and $g_m(r)$ is the analytic solution of

$$g_m''(r) + \frac{2m + 1}{r} g_m'(r) - \left(1 - \frac{f_c^4}{16} r^2\right) g_m + r^{2m} g_m^3 = 0, \quad g_m'(0) = 0, \quad g_m(\infty) = 0. \tag{31}$$

Proof. The proof of Lemma 7 is identical to the proof of Lemma 3 in Appendix B. □

A systematic study of Eq. (29) was conducted in [8, Section 4] for the case $m = 0$. We now present a similar study for the case $m > 0$.

Solutions of Eq. (29) depend on the parameters f_c and g_0 , see Lemma 7.

Lemma 8. All solutions of (29) are decaying as $\rho \rightarrow \infty$. Moreover,

$$G_m(\rho) \sim \frac{c_G}{\rho} \cos\left(\frac{f_c^2}{8} \rho^2 - \frac{2}{f_c^2} \log \rho\right) + \mathcal{O}\left(\frac{1}{\rho^2}\right), \quad \rho \rightarrow \infty. \tag{32}$$

Proof. The result was proved in [20, Theorem 1.1] for the case $m = 0$. The proof for $m > 0$ is identical. □

Lemma 8 implies that for any choice of f_c and g_0 the solutions of (29) are decaying as $\rho \rightarrow \infty$, and that G_m has an oscillatory tail of magnitude c_G . Fig. 3 shows solutions of Eq. (29) with $f_c = 0.35$ for various values of g_0 . In general, these solutions can be separated into two regions:

- (1) A ring region, in which G_m is positive with one or several rings.
- (2) A tail of decaying-to-zero oscillations (in accordance with Lemma 8).

The tails of the solutions in Fig. 3 are of significant magnitude. Clearly, we are interested in solutions of the G_m equation that look as in Fig. 1 and not as in Fig. 3, i.e., without the oscillatory tail. Since the amplitude of the decaying oscillations is governed by c_G , see Eq. (32), we can equivalently say that we are interested in ring solutions of Eq. (29) with the smallest-possible tail (i.e., c_G). Therefore, following [8] we define the single-ring profile of Eq. (29) with a given value of f_c as the single-ring solution with the value of g_0 that gives rise to the smallest-possible value c_G . More generally, the k -ring profile is the k -ring solution of (29) with the minimal value of c_G .⁴ Fig. 4 shows a graph of the tail magnitude c_G as a function of g_0 for $m = 2$ and $f_c = 0.35$. In general, c_G is $\mathcal{O}(1)$, but it sharply falls into minimum points at several locations.⁵ Let us denote the values of g_0 at the minimum points by, going from left to right, $g_0^{(1)}, g_0^{(2)}, g_0^{(3)}, \dots$. Plotting the corresponding G_m profiles shows that $g_0 = g_0^{(k)}$ corresponds to a k -ring profile (see Fig. 5), which we denote by $G_{m,k}$. Let us denote by $g_0^{(k)}(f_c)$ the value of g_0 for which the solution of Eq. (29) is a k -ring profile, according to the above definition of ring profiles. Therefore, Eq. (29) gives rise to one-parameter families of k -ring profiles which are determined by $(f_c, g_0^{(k)}(f_c))$. As g_0 decreases, the ring radius r_{\max} , i.e. the location of its peak, increases. Therefore, the family of k -ring vortices can also be parameterized by the vortex radius, see Fig. 6(A).

Lemma 8 implies that all solutions of Eq. (29) have infinite power (L^2 norm) due to the slowly decaying oscillatory tail. Note that, in particular, this is true for the k -ring solutions of Eq. (29), since, in this case, the value of c_G is small but not zero. Therefore, the explicit blowup solutions $\psi_{G_m}^{\text{explicit}}$ are not in H^1 .

In Section 4.6.4 we will see that it makes sense to consider the G profile only in the ring region, and to define the power of ψ_G as the power in the ring region. One possible definition for the transition point $\rho_{\text{transition}}$ between the ring region and the tail region is where the coefficient of G_m in (29) changes sign. In this case we denote,

$$P_{\text{ring}} = \int_0^{\rho_{\text{transition}}} |\psi_{G_m}|^2 \rho \, d\rho, \tag{33}$$

⁴ The minimal value of c_G can be close to, but not equal to, zero (see Fig. 4). Indeed, from Lemma 8 it follows that if $c_G = 0$ then $G_m \equiv 0$. Therefore, a k -ring solution of (29) does have an oscillating tail, but its magnitude is minimal.

⁵ Other choices of m and f_c give rise to the same qualitative picture (data not shown).

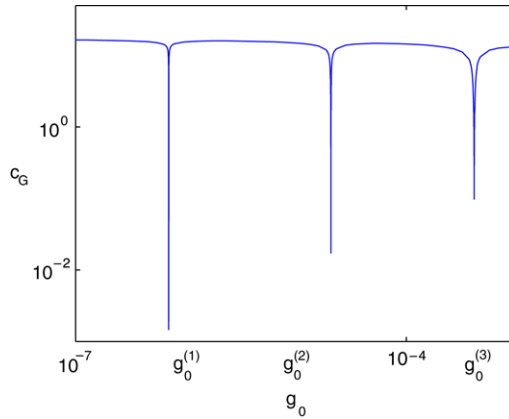


Fig. 4. Graph of c_G as a function of g_0 for $m = 2$ and $f_c = 0.35$.

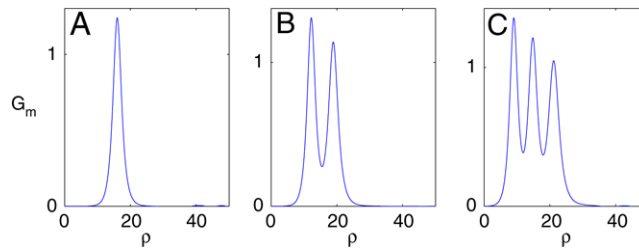


Fig. 5. Solutions of (29) with $m = 2$ and $f_c = 0.35$. A: single-ring solution with $g_0 = g_0^{(1)} \approx 6.99 \times 10^{-7}$. B: double-ring solution with $g_0 = g_0^{(2)} \approx 2.07 \times 10^{-5}$. C: triple-ring solution $g_0 = g_0^{(3)} \approx 4.14 \times 10^{-4}$.

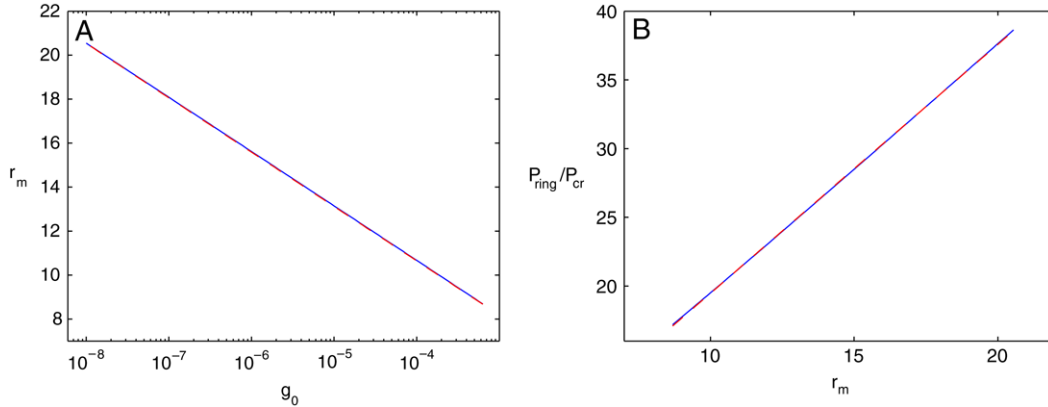


Fig. 6. Single-ring solutions of Eq. (29) with $m = 2$ and initial condition g_0 varying between 10^{-8} and 6×10^{-4} . A: Ring radius r_{\max} as a function of g_0 on a semi-logarithmic scale. The dashed curve is the fitted line $r_{\max} \approx 1.95e^{-1.07g_0}$. The two lines are indistinguishable. B: Normalized ring power $P_{\text{ring}}/P_{\text{cr}}$ as a function of r_{\max} . Dashed curve is the fitted line $P_{\text{ring}}/P_{\text{cr}} \approx 3.85e^{1.81r_{\max}}$. The two lines are indistinguishable.

where $\rho_{\text{transition}} = \frac{2\sqrt{2+\sqrt{4+f_c^4 m^2}}}{f_c^2}$ is the solution of $1 + \frac{m^2}{\rho^2} - \frac{f_c^4}{16}\rho^2 = 0$. Recall, that as g_0 decreases the vortex radius increases. Hence, its power increases. Therefore, the family of k -ring vortices can also be parameterized by the vortex ring power P_{ring} , see Fig. 6(B).

The phase of the explicit blowup solutions $\psi_{G_m}^{\text{explicit}}$ at a given rescaled radius $\rho = r/L(t)$ is

$$\theta(t) = -\frac{1}{m} \int_0^t \frac{ds}{L^2(s)} - \frac{LL_t}{4m} \rho^2 = \theta(0, \rho) - \tilde{\theta}(t), \tag{34}$$

where

$$\theta(0, \rho) = \frac{f_c^2}{8m} \rho^2, \quad \tilde{\theta}(t) = \frac{1}{m} \int_0^t \frac{ds}{L^2(s)} = \frac{1}{mf_c^2} \log\left(\frac{1}{T_c - t}\right).$$

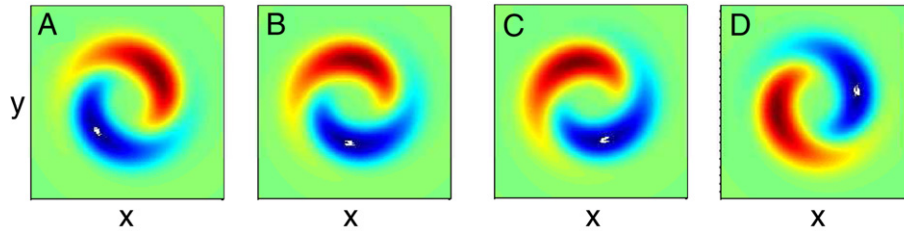


Fig. 7. $\text{Im} \left[R_{m=1, k=0}(\rho) e^{i\theta + i\tau + \frac{f_c^2}{8} \rho^2} \right]$ with $f_c = 1.75$ and $T_c = 1$ at A: $1/L = 1$ ($t = 0$), B: $1/L = 5$ ($t \approx 0.96$), C: $1/L = 10$ ($t \approx 0.990$), D: $1/L = 100$ ($t \approx 0.999$).

The phase is composed of a radially-dependent spiral term $\theta(0, \rho)$ whose value depends on f_c , and a uniform phase term $-\tilde{\theta}(t)$. Note that, unlike $\psi_{R_m}^{\text{explicit}}$, the phase distortion remains constant for all $t > 0$, see Fig. 7.

4.3. Critical power for collapse $P_{\text{cr}}(m)$

The minimal power for collapse in the critical NLS was found by Weinstein [21]:

Theorem 9. Let ψ be a solution of the critical NLS (4) whose initial condition ψ_0 is in H^1 . Then, a necessary condition for collapse is that $\|\psi_0\|_2^2 \geq P_{\text{cr}}$, where $P_{\text{cr}} = \|R\|_2^2$ is the power of the ground state of (5).

The result of Theorem 9 is valid for any initial condition. We now generalize this result for the special case of vortex initial conditions:

Theorem 10. Let ψ be a solution of the critical NLS (4) whose initial condition ψ_0 is a vortex profile (7) with winding number m . Then, a necessary condition for collapse is that $\|\psi_0\|_2^2 \geq P_{\text{cr}}(m)$, where $P_{\text{cr}}(m) = \|R_{m,0}\|_2^2$ is the power of the ground state of (18).

Corollary 11. A necessary condition for collapse in Eq. (17) is that $\|A_0\|_2^2 \geq P_{\text{cr}}(m)$.

The proof of Theorem 10 uses Hamiltonian conservation together with the appropriate Gagliardo–Nirenberg inequality to find an a priori bound for $\|\nabla\psi\|_2^2$. At the heart of the proof are the following Lemmas:

Lemma 12. Let $J_m[f]$ be given by

$$J_m[f] = \frac{\|\nabla f\|_2^2 \|f\|_2^2}{\|f\|_4^4} + m^2 \frac{\|f/r\|_2^2 \|f\|_2^2}{\|f\|_4^4}. \quad (35)$$

Then, $\inf_{f \in \mathcal{F}} J_m[f]$ is attained, where \mathcal{F} is defined in (10).

Proof. See Appendix D. \square

Lemma 13. The optimal constant C_m in the Gagliardo–Nirenberg inequality

$$\|f_m\|_4^4 \leq C_m \|\nabla f_m\|_2^2 \|f_m\|_2^2, \quad (36)$$

where

$$f_m = f(r) e^{im\theta} \in H^1, \quad (37)$$

is given by $C_m = 2/\|R_{m,0}\|_2^2$, where $R_{m,0}$ is the ground state solution of (18).

Proof. The optimal constant C_m is given by

$$C_m = \frac{1}{\inf_{0 \neq f(r) e^{im\theta} = f_m \in H^1} J[f_m]}, \quad J[f_m] = \frac{\|\nabla f_m\|_2^2 \|f_m\|_2^2}{\|f_m\|_4^4}. \quad (38)$$

Since $J[f_m = e^{im\theta} f(r)] = J_m[f]$ and since the infimum of $J_m[f]$ is attained (Lemma 12),

$$C_m = \frac{1}{\inf_{0 \neq f \in \mathcal{F}} J_m[f]} = \frac{1}{\min_{0 \neq f \in \mathcal{F}} J_m[f]}. \quad (39)$$

To finish the proof, we find the extremals of $J_m[f]$ and show that $R_{m,0}$ minimizes $J_m[f]$, see Appendix E. \square

Table 1

Critical power $P_{cr}(m) = \int_0^\infty |R_{m,0}|^2 r dr$

m	1	2	3	4	5	6	7	8	9	10
$P_{cr}(m)$	7.68	14.26	21.05	27.90	34.78	41.67	48.57	55.48	62.45	69.14

Proof of Theorem 10. Following [21], from the conservation of the Hamiltonian and of the power, and from the Gagliardo–Nirenberg inequality (36), it follows that

$$\|\nabla\psi\|_2^2 \leq H(0) + \frac{C_m}{2} \|\psi_0\|_2^2 \|\nabla\psi\|_2^2, \tag{40}$$

for $\psi = A(t, r)e^{im\theta} \in H^1$. A sufficient condition for global existence, i.e., for $\|\nabla\psi\|$ to be bounded, is $\frac{C_m}{2} \|\psi_0\|_2^2 < 1$. Hence

$$P_{cr}(m) = \frac{2}{C_m}. \tag{41}$$

By Lemma 13, $\frac{2}{C_m} = \|R_{m,0}\|_2^2$. Hence, $P_{cr}(m) = \|R_{m,0}\|_2^2$. \square

Remark 14. The result of Theorem 10 is sharp in the sense that singular vortex solutions with initial condition $\psi_0 = A_0(r)e^{im\theta}$ with power less than $P_{cr}(m)$ do not exist, but singular vortex solutions with exactly the power $P_{cr}(m)$ ($\psi_{R_{m,0}}^{\text{explicit}}$) do exist.

The critical power $P_{cr}(m)$ can also be defined as the minimal power of all vortex profiles with a non-positive Hamiltonian:

Corollary 15.

$$P_{cr}(m) = \min_{0 \neq \psi_0 = f(r)e^{im\theta} \in H^1} \left\{ \|\psi_0\|_2^2 \mid H(\psi_0) \leq 0 \right\}. \tag{42}$$

Proof. From (40) and (41) it follows that

$$\frac{P_{cr}(m) - \|\psi_0\|_2^2}{P_{cr}(m)} \|\nabla\psi_0\|_2^2 \leq H(\psi_0).$$

Hence, if $H(\psi_0) \leq 0$ then $\|\psi_0\|_2^2 \geq P_{cr}(m)$. Therefore,

$$P_{cr}(m) \leq \inf_{0 \neq \psi_0 = f(r)e^{im\theta} \in H^1} \left\{ \|\psi_0\|_2^2 \mid H(\psi_0) \leq 0 \right\}.$$

Since $H(R_{m,0}e^{im\theta}) = 0$ and $\|R_{m,0}e^{im\theta}\|_2^2 = P_{cr}(m)$, the result follows. \square

Theorem 10 shows that the critical power $P_{cr}(m)$ increases with m :

Corollary 16. $P_{cr}(m)$ is monotonically increasing in m , i.e.,

$$P_{cr}(0) < P_{cr}(1) < P_{cr}(2) < \dots$$

Proof. By (35), (39) and (41), $P_{cr}(m) = 2 \min_{f \in \mathcal{F}} J_m[f] = 2 \min_{f \in \mathcal{F}} \left[\frac{\|\nabla f\|_2^2 \|f\|_2^2}{\|f\|_4^4} + m^2 \frac{\|f/r\|_2^2 \|f\|_2^2}{\|f\|_4^4} \right]$. Since for any f the functional $J_m[f]$ is monotonically increasing in m , $P_{cr}(m)$ is also monotonically increasing in m . \square

The value of $P_{cr}(m) = \int |R_{m,0}|^2 r dr$ for $m = 1, \dots, 10$ is listed in Table 1. We can also derive an analytic approximation for $P_{cr}(m)$ by using the approximation (19):

$$P_{cr}(m) = \int_0^\infty |R_{m,0}|^2 r dr \approx 3 \int_0^\infty \operatorname{sech}^2 \left(\frac{r - \sqrt{2}m}{\sqrt{2/3}} \right) r dr \quad r = 2 \log(e^{2\sqrt{3}m} + 1).$$

Therefore, $P_{cr}(m) \approx 4\sqrt{3}m$, for $m \gg 1$.

Fig. 8 shows that the critical power is well approximated by $4\sqrt{3}m$, and that the approximation improves as m increases. Already for $m = 2$ the approximation error is less than 3%, and for $m \geq 5$ the error is below 0.4%.

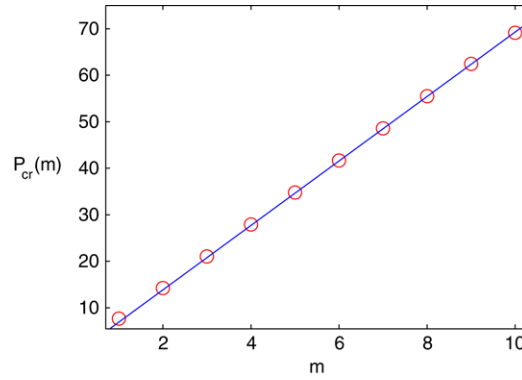


Fig. 8. Critical power $P_{cr}(m) = \int_0^\infty |R_{m,0}|^2 r dr$ as a function of m (o). The solid line is $4\sqrt{3}m$.

Table 2
 $P_{th}^{(m)}[f]$ for various input profiles

m	Input profile (f)		
	Laguerre-Gaussian (Eq. (44))	sech (Eq. (45))	“Modified” sech (Eq. (48))
1	7.73 (+0.65%)	9.19 (+19.66%)	7.69 (+0.13%)
2	14.66 (+2.80%)	14.9 (+4.48%)	14.39 (+0.91%)
3	22.52 (+7%)	21.44 (+1.9%)	21.20 (+0.71%)
4	30.97 (+11%)	28.71 (+2.9%)	27.99 (+0.32%)
5	39.65 (+14%)	37.92 (+9%)	34.84 (+0.17%)
6	49.60 (+19%)	47.52 (+14%)	41.81 (+0.34%)
7	59.27 (+22%)	57.49 (+18%)	48.68 (+0.23%)
8	69.69 (+26%)	69.19 (+25%)	55.53 (+0.09%)
9	80.56 (+29%)	84.28 (+35%)	62.51 (+0.1%)
10	91.96 (+33%)	97.90 (+30%)	69.20 (+0.09%)

The value in parentheses is $(P_{th}^{(m)} - P_{cr}(m))/P_{cr}(m)$.

4.3.1. Threshold power for collapse

Let us consider the one-parameter family of initial conditions

$$\psi_0 = c f(r) e^{im\theta}, \tag{43}$$

for the critical NLS (4). Since $H(\psi_0) = c^2 [H(f e^{im\theta}) - (c^2 - 1) \|f\|_4^4]$, there exists a threshold value $c_H = c_H(f)$ such that for all $c > c_H$, $H(\psi_0) < 0$ and hence by the variance identity (6), the solution becomes singular. Therefore, there exists a threshold value $c_{th} \leq c_H$, such that the critical NLS solution with initial condition (43) becomes singular if $c > c_{th}$, or, equivalently, if $\|\psi_0\|_2^2 > P_{th}^{(m)}[f] = c_{th}^2 \|f\|_2^2$. Therefore, $P_{th}^{(m)}[f]$ is the threshold power for collapse for the initial condition (43). By Theorem 10, $P_{cr}(m) \leq P_{th}^{(m)}[f] \leq P(c_H f)$.

In the case of non-vortex solutions ($m = 0$), Merle [22,23] showed that if $f \not\equiv R_{0,k=0}^\lambda$, then $P_{th}^{(m)}[f] > P_{cr}$. Numerical simulations suggested that the threshold power for collapse of radially-symmetric initial conditions is usually only a few percent above the critical power $P_{cr} = P_{cr}(m = 0)$ [24]. For example, the threshold power of Gaussian input beams of the form $\psi = c e^{-r^2}$ is $P_{th}^{(m=0)} = 1.017 P_{cr}$.

We now consider the threshold power of various vortex initial conditions, and ask under what condition the threshold power is close to the critical power $P_{cr}(m)$. Of course, when $f = R_{m,0}$ then $P_{th}[f] = P_{cr}(m)$ since $P_{cr}(m) = P(f)$ and $H(f e^{im\theta}) = 0$. We now calculate the threshold power of the Laguerre-Gaussian profiles

$$f = c r^m e^{-r^2}, \tag{44}$$

which are the vortex modes of the linear Schrödinger equation. To do that, we solve the NLS with the initial condition (44) and gradually increase c until, at c_{th} , the solution collapses. In this case, the threshold power $P_{th}^{(m)}[f]$ is close to the critical power $P_{cr}(m)$ for $m = 1$ but as m increases, the threshold power $P_{th}^{(m)}[f]$ increases faster than the critical power, see Table 2. Similarly, in the case of the input profile

$$f = c r^2 \operatorname{sech}(r - 5), \tag{45}$$

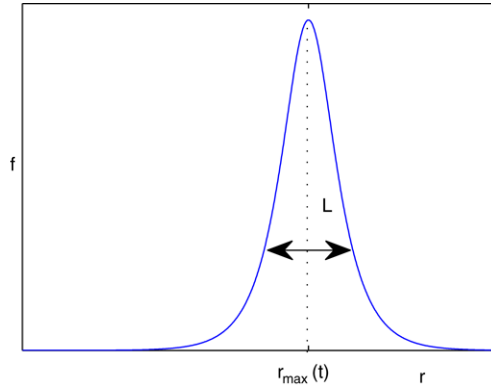


Fig. 9. Illustration of ring radius r_{\max} and width L .

the threshold power is close to $P_{\text{cr}}(m)$ only for $m = 2, 3, 4$, see Table 2. Note that the r^2 term ensures that the profile vanishes at $r = 0$.

To understand these observations, we note that from the definition of c_H , one can derive the relation [6] $P(c_H f) = 2J_m[f]$, where J_m is given by (35). In addition, from (39) and (41) we have that $2J_m[R_{m,0}^\lambda] = P_{\text{cr}}(m)$. Therefore, we see that $2J_m[R_{m,0}^\lambda] \leq P_{\text{th}}^{(m)}[f] \leq 2J_m[f]$. Hence, the closer f is to $\{R_{m,0}^\lambda\}_{\lambda \in R^+}$ in H^1 , the closer $P_{\text{th}}^{(m)}[f]$ is to $P_{\text{cr}}(m)$.

To estimate the distance between f and $\{R_{m,0}^\lambda\}_{\lambda \in R^+}$ in H^1 , let us consider a profile of the form

$$f = Q\left(\frac{r - r_{\max}}{L}\right), \tag{46}$$

where $Q(\rho)$ attains its maximum at $\rho = 0$. This profile is characterized by the width L and the radius r_{\max} , see Fig. 9. By (20), the family $\{R_{m,k}^\lambda\}_{\lambda \in R^+}$ is characterized by

$$\text{radius/width} = r_{\max}^\lambda / L^\lambda = \sqrt{3}m. \tag{47}$$

Therefore, for a profile ψ_0 of the form (43), where f is of the form (46), to be “close” to the family $\{R_{m,k}^\lambda\}_{\lambda \in R^+}$, f has to satisfy (47) to “leading order”.

The Laguerre-Gaussian modes (44) are characterized by $\text{radius/width} = \sqrt{m/2}$. This ratio is close to (47) only for $m \approx 1$, explaining why the threshold power of Laguerre-Gaussian modes is close to $P_{\text{cr}}(m)$ only for $m = 1$. Similarly, the sech profile (45) is characterized by $\text{radius/width} = 5$. Since the radius/width of $R_{m,0}^\lambda$ is equal to $\sqrt{3}m$, the ratio is close to 5 for $m = \frac{5}{\sqrt{3}} \approx 2.88$, see Eq. (47). This explains why the threshold power of the sech profile (45) is closest to $P_{\text{cr}}(m)$ for $m = 3$.

We can “fix” the sech profile (45) so that “it behaves like the $R_{m,0}^\lambda$ profile”, i.e., it satisfies (47) to leading order, as follows:

$$f = \sqrt{2} \left(\frac{r}{\sqrt{3}m}\right)^2 \text{sech}\left(r - \sqrt{3}m\right). \tag{48}$$

Indeed, the threshold power of the “modified” sech profile (48) is less than 1% above the critical power for $m = 1, \dots, 10$, see Table 2.

Therefore, we conclude that the threshold power of initial conditions of the form (46) is close to the critical power only for profiles that are close to $R_{m,0}^\lambda$ in the ring region, i.e., those that satisfy (47) “to leading order”. Note, in particular, that the profile of the initial condition outside the ring region has a minor effect on the threshold power. For example, the threshold power of the “modified” sech profile (48) is closest to the critical power at $m = 3$, even though $R_{m=3,0}^\lambda \sim cr^3$ near the origin $r = 0$, while the “modified” sech profiles behave as r^2 near the origin.

4.3.2. Kruglov’s estimate of the critical power

In [3], Kruglov and Logvin estimated the critical power for vortex collapse by assuming that the vortex solution collapses with a self-similar Laguerre-Gaussian profile

$$\psi_Y(z, r, \theta) = \frac{1}{L} Y\left(\frac{r}{L}\right) e^{i\tau + im\theta + i\frac{L_z}{L} \frac{r^2}{4}}, \quad \tau = \int_0^t \frac{ds}{L^2(s)}, \quad L = \sqrt{T_c - t}, \tag{49}$$

where $Y(r) = cr^m e^{-\eta r^2}$.

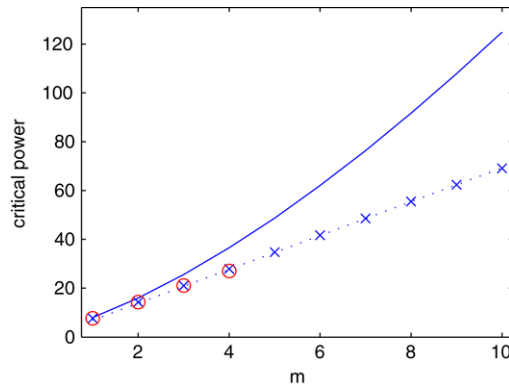


Fig. 10. Numerical estimate of the critical power (o) (data taken from [3]), analytic estimate $I_{cr}^{(m)}$, see Eq. (50) (solid curve), critical power $P_{cr}(m) = \int_0^\infty |R_{m,0}|^2 r dr$, denoted by (x). The dotted line is $4\sqrt{3}m$.

The parameters c and η were determined from the condition that Y is an extremal of the averaged action integral

$$S = \int_0^\infty \tilde{\mathcal{L}}\left(\frac{dY}{dr}, Y\right) r dr, \quad \tilde{\mathcal{L}} = \int_{t=-\infty}^\infty \int_{\theta=0}^{2\pi} \mathcal{L}\left(\frac{d\psi}{dr}, \frac{d\psi}{d\theta}, \frac{d\psi}{dt}, \psi\right) d\theta dt,$$

where \mathcal{L} is the Lagrangian of the NLS (4) and $\tilde{\mathcal{L}}$ is the averaged Lagrangian. Based on this calculation, the critical power was determined by Kruglov and Logvin to be equal to

$$I_c^{(m)} = \frac{2^{2m+1} m!(m+1)!}{(2m)!}. \tag{50}$$

In [3], Kruglov and Logvin also estimated the critical power numerically for $m = 1, 2, 3$ and 4. The numerical results in [3] agree with our analytic calculation of $P_{cr}(m)$, but not with his estimate $I_c^{(m)}$, see Fig. 10. To understand why this is the case, we note that the derivation of $I_c^{(m)}$ is based on the following two assumptions:

- (1) The collapsing vortex is a self-similar solution.
- (2) The self-similar blowup profile is a Laguerre-Gaussian mode.

The first assumption is equivalent to the assumption that the variance $V = \int |x|^2 |\psi|^2 dx$ vanishes exactly at the singularity point. From the variance identity (6), this can occur only if $H(Y) \leq 0$. Indeed, the critical power estimate (50) can be immediately obtained from the condition $H(Y) = 0$, since

$$H(Y) = 0 \implies \frac{c}{\sqrt{\eta}} = 2^{m+1} \sqrt{\frac{2^{m+1} m!(m+1)!}{(2m)!}} \implies \|\psi_Y\|_2^2 = \frac{2^{2m+1} m!(m+1)!}{(2m)!}.$$

Hence, the critical power estimate $I_c^{(m)}$ can be reformulated as

$$I_c^{(m)} = \inf \left\{ \|Y\|_2^2 \mid Y = cr^m e^{-\eta r^2} \neq 0, H(Y e^{im\theta}) \leq 0 \right\}. \tag{51}$$

In Corollary 15, we showed that the critical power $P_{cr}(m)$ can be defined by (42). Therefore, the critical power estimate (51) can be viewed as (42) with the additional constraint $Y = cr^m e^{-\eta r^2}$. Since the minimum of (42) is attained by $R_{m,0}^\lambda$, the estimate $I_c^{(m)}$ can be close to $P_{cr}(m)$ only if the test function Y is close to the minimizers $R_{m,0}^\lambda$. However, in Section 4.3.1 we saw that Laguerre-Gaussian modes are not a good approximation of $R_{m,0}^\lambda$ and that as m increases this approximation becomes less and less accurate. Indeed, Fig. 10 shows that the estimate $I_c^{(m)}$ is closest to $P_{cr}(m)$ for $m = 1$ and becomes less and less accurate as m increases.

4.3.3. Critical power for non-radial vortex initial conditions

Theorem 10 holds only for initial conditions of the form $\psi_0 = A_0(r)e^{im\theta}$, or equivalently for any initial condition of (17). In contrast, non-radial vortex initial conditions (i.e., those for which A_0 is not radially-symmetric) can collapse with power only slightly above $P_{cr}(0)$, hence with power significantly below $P_{cr}(m)$:

Lemma 17. *Let $\varepsilon > 0$. Then, there exists $\psi_0 = A_0(x, y)e^{im\theta}$ where A_0 is a real function such that $\|\psi_0\|_2^2 < P_{cr}(0) + \varepsilon$ and the solution of the critical NLS (4) with the initial condition ψ_0 becomes singular in a finite time.*

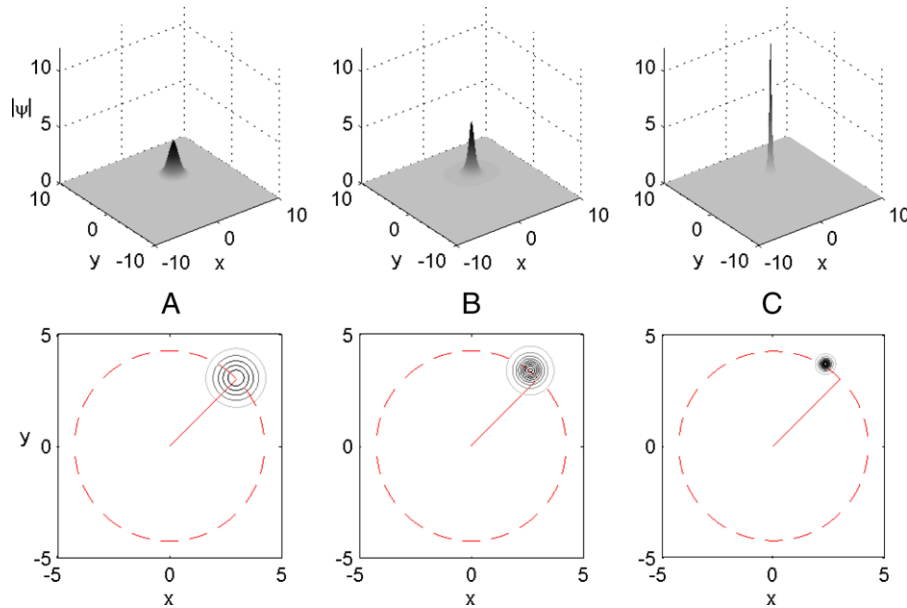


Fig. 11. Solution of the NLS (4) with initial condition (52) at A: $t = 0$, B: $t = 0.54$, C: $t = 1$. The dashed curve is the circle $x^2 + y^2 = 3^2$. The solid line connects the origin with the center of mass of the initial condition.

Proof. Let $\mathbf{x} = (x, y)$ and let $\psi_0 = (1 + \varepsilon)u(\mathbf{x}; \mathbf{x}_0)e^{im\theta}$ where $u(\mathbf{x}; \mathbf{x}_0) = v(|\mathbf{x}|)R(\mathbf{x} - \mathbf{x}_0)$, $R_{m=0,0}$ is the ground state of (5), and v is a smooth function that behaves like $|x|^m$ near $x = 0$, is monotonically increasing in $|x|$ and is identically one outside the unit circle. The Hamiltonian of ψ_0 is given by

$$\begin{aligned} H(\psi_0) &= H((1 + \varepsilon)u(\mathbf{x}; \mathbf{x}_0)) + (1 + \varepsilon)^2 m^2 \left\| \frac{u(\mathbf{x}; \mathbf{x}_0)}{|\mathbf{x}|} \right\|_2^2 \\ &= (1 + \varepsilon)^2 \|\nabla u(\mathbf{x}; \mathbf{x}_0)\|_2^2 - (1 + \varepsilon)^4 \|u(\mathbf{x}; \mathbf{x}_0)\|_4^4 + \frac{(1 + \varepsilon)^2 m^2}{|\mathbf{x}_0|^2} \left\| \frac{u(\mathbf{x})}{|1 + \frac{\mathbf{x}}{\mathbf{x}_0}|} \right\|_2^2 \\ &= (1 + \varepsilon)^2 \left[H(u(\mathbf{x}; \mathbf{x}_0)) - \varepsilon(2 + \varepsilon) \|u(\mathbf{x}; \mathbf{x}_0)\|_4^4 \right] + \frac{(1 + \varepsilon)^2 m^2}{|\mathbf{x}_0|^2} \left\| \frac{u(\mathbf{x})}{|1 + \frac{\mathbf{x}}{\mathbf{x}_0}|} \right\|_2^2. \end{aligned}$$

Since for a fixed ε , $\lim_{|\mathbf{x}_0| \rightarrow \infty} \frac{1}{|\mathbf{x}_0|^2} \left\| \frac{u(\mathbf{x})}{|1 + \frac{\mathbf{x}}{\mathbf{x}_0}|} \right\|_2^2 = 0$ and $\lim_{|\mathbf{x}_0| \rightarrow \infty} H(u(\mathbf{x}; \mathbf{x}_0)) = H(R_{m=0,0}) = 0$, it follows that for large enough values of $|\mathbf{x}_0|$, $H(\psi_0) < 0$ and hence by the variance identity (6) the solution collapses. Since, in addition $\lim_{|\mathbf{x}_0| \rightarrow \infty} \|\psi_0\|_2^2 = (1 + \varepsilon)^2 P_{\text{cr}}(0)$, the result follows. \square

To demonstrate numerically the result of Lemma 17, we solve the NLS (4) with the initial condition

$$\psi_0 = 2.8 \frac{-(x-3)^2 - (y-3)^2}{\exp} \tanh^2(4x^2 + 4y^2) e^{i2\theta}, \tag{52}$$

whose power is $\|\psi_0\|_2^2 \approx 1.05 P_{\text{cr}}(0) \approx \frac{1}{7} P_{\text{cr}}(2)$. In Fig. 11 we see that the corresponding solution undergoes collapse. Therefore, this confirms that non-radial vortex initial conditions with power slightly above $P_{\text{cr}}(0)$, hence with power significantly below $P_{\text{cr}}(m)$, can collapse.

The difference between Theorem 10 and Lemma 17 is due to the location of the collapse point. In the case of Theorem 10, because of radial symmetry, the collapse point has to be at the origin. Since the vorticity “forces” the solution to behave as r^m near the origin (see Lemma 3), it cannot collapse with the R profile, but only with the R_m profile.⁶ “As a result”, the critical power for collapse increases from $P_{\text{cr}}(0)$ to $P_{\text{cr}}(m)$. However, when the collapse point is not at $r = 0$, the vorticity does not prohibit the solution from collapsing with the R profile since locally near the collapse point $\mathbf{x}_c = r_c e^{im\theta_c} \neq 0$ the vorticity only “adds” a constant phase term $e^{im\theta_c}$, hence the critical power for collapse at \mathbf{x}_c is $P_{\text{cr}}(0)$. This intuitive explanation agrees with previous observations that the critical power is determined only by the local properties near the collapse point. Thus, for example, in the inhomogeneous NLS, $i\psi_t + \Delta\psi + k(\mathbf{x})|\psi|^2\psi = 0$ the critical power for collapse at \mathbf{x}_c depends only on $k(\mathbf{x}_c)$ [25], and the critical power for collapse for the NLS (4) on bounded domains is the same as in free space [26].

⁶ See also Section 4.6.1.

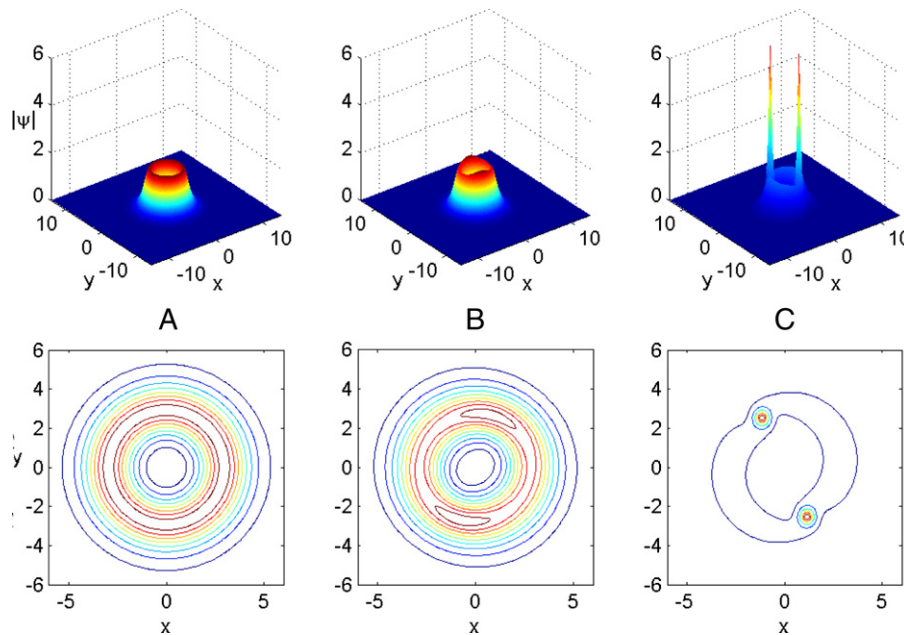


Fig. 12. Solution of the critical NLS (4) with slightly elliptic initial condition (53) at A: $t = 0$, B: $t = 2.19$, C: $t = 3.45$.

So far we only considered the collapse of non-radial vortex solutions whose “center of mass” is far from the origin. We now show that non-radial vortex solutions whose center of mass is at $r = 0$ can also collapse with power below $P_{cr}(m)$. In Fig. 12 we solve the NLS (4) with the slightly elliptic initial condition

$$\psi_0 = 0.98R_2 \left(\sqrt{x^2 + (1.01 \cdot y)^2} \right) e^{i2\theta}, \tag{53}$$

whose power is $\|\psi_0\|_2^2 \approx 0.95P_{cr}(2)$. In this case, the center of mass of the solution $\bar{\mathbf{x}}(t) = \frac{1}{\|\psi\|_2^2} \int \mathbf{x}|\psi|^2$ remains at $\mathbf{x} = 0$ for all t . Indeed,

Lemma 18. *Let ψ be a vortex solution of the NLS with an initial condition of the form $\psi_0 = A_0(x, y) e^{im\theta}$, where A_0 is real and*

$$A_0(-x, y) = A_0(x, y) = A_0(x, -y) = A_0(-x, -y). \tag{54}$$

Then, $\bar{\mathbf{x}}(t) \equiv 0$.

Proof. See Appendix F. \square

Because the ring is azimuthally unstable (see Section 4.6.6), it breaks into two filaments which subsequently undergo collapse. The center of each of these filaments is not at $r = 0$, and therefore each of them collapses with the critical power $P_{cr}(0)$. Note that when A_0 satisfies condition (53) or (54) and m is even, the initial condition is symmetric under the transformation $(x, y) \rightarrow (-x, -y)$. Hence, the NLS solution preserves this symmetry for all $t > 0$. Therefore, filaments which are not at the origin must appear in pairs which are symmetric with respect to the origin, as can be seen in Fig. 12. In this case, the critical power for collapse is at least $2P_{cr}(0)$.

4.4. Blowup instability of stationary vortex solutions

The instability of stationary vortex solutions was proved for the supercritical case in [15–17]. We now prove that in the critical case, stationary vortex solutions are also unstable. We begin with the following Lemma:

Lemma 19. *Let*

$$\psi_{m,k}^{\text{stationary}} = e^{it} R_{m,k}(r) e^{im\theta}, \tag{55}$$

where $R_{m,k}$ is a solution of Eq. (18) with k nodes in $(0, \infty)$. Then,

- (1) *For any k , the Hamiltonian of $\psi_{m,k}^{\text{stationary}}$ is zero, i.e., $H(\psi_{m,k}^{\text{stationary}}) = 0$.*
- (2) *$\psi_{m,k=0}^{\text{stationary}}$ has exactly the critical power, i.e., $\|\psi_{m,k=0}^{\text{stationary}}\|_2^2 = P_{cr}(m)$.*

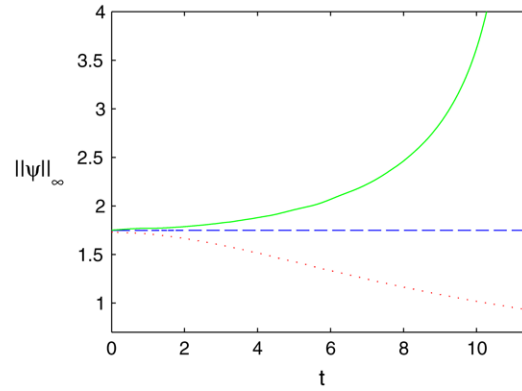


Fig. 13. Solution of the critical NLS (4) for the initial conditions (56) for $\varepsilon = 0$ (dashed), $\varepsilon = -0.01$ (dots), and $\varepsilon = 0.01$ (solid).

Proof. (1) Since $V(\psi_{m,k}^{\text{stationary}}(t)) \equiv V(\psi_{m,k}^{\text{stationary}}(t = 0))$, it follows from the variance identity (6) that $0 = \frac{1}{8} V_{tt} = H(\psi_{m,k}^{\text{stationary}})$.
 (2) From Theorem 10, $\|\psi_{m,0}^{\text{stationary}}\|_2^2 = \|R_{m,0}\|_2^2 = P_{\text{cr}}(m)$. \square

The following lemma shows that the critical stationary vortex solutions $\psi_{m,k}^{\text{stationary}}$ are strongly unstable:

Lemma 20. Let $\psi_{m,k}^{\text{stationary}}$ be a stationary vortex solution (55) of the critical NLS (4). Then, $\psi_{m,k}^{\text{stationary}}$ is strongly unstable, i.e., for any $\varepsilon > 0$, the NLS solution with initial condition

$$\psi_0 = (1 + \varepsilon)\psi_{m,k}^{\text{stationary}}(t = 0), \tag{56}$$

blows up at a finite time.

Proof. The Hamiltonian of ψ_0 is $H(\psi_0) = (1 + \varepsilon)^2 [H(R_{m,k}) - \varepsilon(2 + \varepsilon)\|R_{m,k}\|_4^4]$.

Since $H(R_{m,k}) = 0$, $H(\psi_0) = -\varepsilon(1 + \varepsilon)^2(2 + \varepsilon)\|R_{m,k}\|_4^4 < 0$. Therefore, by the variance identity (6), ψ blows up at a finite time. \square

As noted in Section 3, Mizumachi [15–17] proved that the stationary vortex solutions $\psi_{m,k}^{\text{stationary}}$ are linearly unstable in the supercritical case. Lemma 20 thus extends this result to the critical case.

In the case of the ground state stationary vortex $\psi_{m,0}^{\text{stationary}}$, the solution of the critical NLS (4) with initial condition (56) with $-1 < \varepsilon < 0$ exists globally and decays with propagation:

Lemma 21. Let ψ be a solution of the critical NLS (4) with initial condition (56) with $-1 < \varepsilon < 0$. Then, ψ exists globally. In addition, for all $2 \leq p < \infty$,

$$\|\psi\|_p^p \leq \frac{C_p}{t^{p-2}}, \quad 0 \leq t < \infty, \tag{57}$$

where C_p is a constant that depends on p .

Proof. Since the power of $R_{m,k=0}$ is exactly the critical power (see Lemma 19),

$$P(\psi_0) = (1 + \varepsilon)^2 P_{\text{cr}}(m) < P_{\text{cr}}(m).$$

Therefore, by Theorem 10, ψ exists globally. The proof of the decay estimate (57) for any initial condition that satisfies $P < P_{\text{cr}}(m)$ is identical to the one given by Weinstein [27] for the case $m = 0$. \square

The results of Lemmas 20 and 21 are illustrated in Fig. 13.

4.5. Instability of the explicit vortex blowup solutions

In the vortex-free case, the explicit blowup solution $\psi_{R_{0,0}}^{\text{explicit}}$ where $R_{0,0}$ is the ground state solution of (5) is unstable, i.e., when slightly perturbed it either exists globally [21] or it may collapse, but not with a linear blowup rate [7]. No such proof exists for the instability of the excited state blowup solutions $\psi_{R_{0,k}}^{\text{explicit}}$ for $k > 0$. However, numerical simulations show that they are unstable and when perturbed, collapse with the $R_{0,0}$ profile. In the case of the explicit ring blowup solutions $\psi_{G_{0,k}}^{\text{explicit}}$, numerical simulations show that multi-ring solutions ($k > 0$) collapse with a self-similar single-ring profile $G_{0,0}$, hence are unstable. The single-ring $\psi_{G_{0,0}}^{\text{explicit}}$ solutions are “stable” in the sense that they collapse with a quasi-self-similar $G_{0,0}$ ring profile at a square-root blowup rate [8].

We now consider the instability of the explicit vortex blowup solutions. In the case of $\psi_{R_{m,0}}^{\text{explicit}}$, where $R_{m,0}$ is the ground state solution of (18), instability can also be proved analytically:

Corollary 22. *Let ψ be a solution of the critical NLS (4), with $\psi_0 = (1 - \varepsilon)\psi_{R_{m,0}}^{\text{explicit}}(t = 0)$, and $0 < \varepsilon < 1$. Then, ψ exists globally.*

Proof. This follows by applying Lemma 21 to the explicit blowup solution $\psi_{R_{m,0}}^{\text{explicit}}$. \square

In Section 4.6.3 we show numerically that if $\psi_0 = (1 + \varepsilon)\psi_{R_{m,0}}^{\text{explicit}}$ then the solution collapses with a self-similar $G_{m,0}$ single-ring profile at a square-root blowup rate. We also observe numerically that the solution collapses with a self-similar $G_{m,0}$ single-ring profile for the perturbed multi-ring solution $\psi_0 = (1 + \varepsilon)\psi_{R_{m,k}}^{\text{explicit}}$ (data not shown) and $\psi_0 = (1 + \varepsilon)\psi_{G_{m,k}}^{\text{explicit}}$. Hence, both $\psi_{R_{m,0}}^{\text{explicit}}$ and the multi-ring vortices $\psi_{G_{m,k}}^{\text{explicit}}$ and $\psi_{R_{m,k}}^{\text{explicit}}$ are unstable. Therefore, the vortex case is similar to the non-vortex case, in the sense that only $\psi_{G_{m,0}}$ is “stable”, but different in the sense that when slightly perturbed, $\psi_{R_{m,k}}$ ($k = 0, 1, \dots$) collapses with a self-similar $R_{0,0}$ profile when $m = 0$ but with a self-similar $G_{m,0}$ profile when $m > 0$.

4.6. Asymptotic blowup profiles of vortex solutions (critical NLS)

4.6.1. Rigorous results

In Section 4.3 we saw that the minimal input power for collapse of vortices in the critical NLS is $P_{\text{cr}}(m)$. We now show that the amount of power that collapses into the singularity point is also at least $P_{\text{cr}}(m)$. To do so, following Weinstein [21], we first prove that near the singularity the solution converges to a self-similar vortex blowup profile:

Theorem 23. *Let ψ be a solution of the critical NLS (4) with vortex initial condition $\psi_0 = A_0(r)e^{im\theta}$ in H^1 , that blows up at a finite distance T_c . Let*

$$L(t) = \|\nabla\psi\|_2^{-1}, \tag{58}$$

and let

$$S(\psi) = L(t)e^{i\gamma(t)}\psi(t, L(t)r, \theta), \quad \gamma(t) \in [0, 2\pi). \tag{59}$$

Then, for any sequence $t_k \rightarrow T_c$, there is a subsequence t_{k_j} such that $S(\psi)(t_{k_j}, r) \rightarrow \Psi(r)$ strongly in L^p for all $2 < p < \infty$. Furthermore, $\|\Psi\|_2^2 \geq P_{\text{cr}}(m)$ where $P_{\text{cr}}(m) = \|R_{m,0}\|_2^2$.

Proof. See Appendix H. \square

Theorem 23 implies that the amount of power that collapses into the singularity is at least the critical power $P_{\text{cr}}(m)^7$:

Theorem 24 (Concentration Theorem). *Under the conditions of Theorem 23, for all $\varepsilon > 0$,*

$$\liminf_{t \rightarrow T_c} \|\psi\|_{L^2(r < \varepsilon)}^2 \geq P_{\text{cr}}(m).$$

Proof. See Appendix I. \square

Therefore ψ undergoes a strong collapse with at least the critical power $P_{\text{cr}}(m)$. In particular, singular vortex solutions of the critical NLS (4) cannot collapse with the $\psi_{R_{0,0}}$ profile whose power is $P_{\text{cr}} < P_{\text{cr}}(m)$.

4.6.2. Two potential attractors

In Section 4.6.1 we showed that that stable singular vortex solutions of the critical NLS collapse with a self-similar profile differently from $\psi_{R_{0,0}}$. We now ask what is the asymptotic blowup profile of H^1 vortex solutions of the critical NLS.

In Section 4.2 we saw that the critical NLS has two families of explicit vortex blowup solutions: $\psi_{R_m}^{\text{explicit}}$ and $\psi_{G_m}^{\text{explicit}}$. However, $\psi_{R_m}^{\text{explicit}}$ are unstable and $\psi_{G_m}^{\text{explicit}}$ have an infinite L^2 norm. Therefore, the asymptotic blowup profile of H^1 vortex solutions is different from $\psi_{R_m}^{\text{explicit}}$ and from $\psi_{G_m}^{\text{explicit}}$.

Let us consider blowup solutions of the critical NLS (4) that have the asymptotic form $\psi(t, r, \theta) \sim \psi_{A_m}(t, r, \theta)$, where ψ_{A_m} is of the form (26). Note that, in contrast to Section 4.2, ψ_{A_m} is now considered as the limiting asymptotic profile and not as an explicit blowup solution, i.e., we do not assume that $\psi \equiv \psi_{A_m}$. Following the analysis in Section 4.2, A_m is the solution of (27) and $\lim_{t \rightarrow T_c} (LL_t)^2 = \beta_0$.

⁷ This is a generalization of the Concentration Theorem of Merle and Tsutsumi [28] and Weinstein [21].

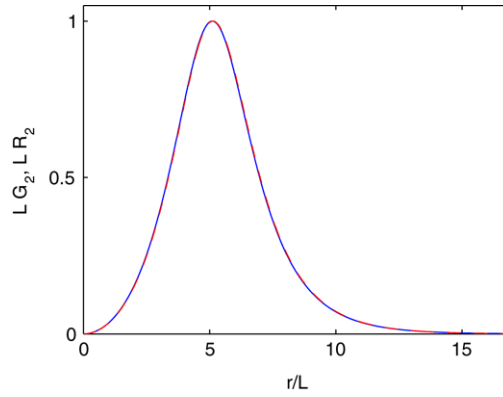


Fig. 14. Solid line: $R_2(r)$. Dashed line: $G_2(r)$ with $f_c = 0.2855$ and $g_0 = 0.1737$. The two lines are indistinguishable.

Therefore, there are two possibilities:

- (1) $\beta_0 = 0$: This is the case of a *faster-than-a-square-root blowup rate*, i.e., $\frac{L(t)}{\sqrt{T_c-t}} \rightarrow 0$. In this case, we denote $A_m(\rho) = R_m(\rho)$, where R_m is the solution of (18).
- (2) $\beta_0 > 0$: In this case the blowup rate is a *square root*, i.e., $L(t) \sim f_c \sqrt{T_c - t}$ where $f_c^2 = \beta_0/2$. In this case, we denote $A_m(\rho) = G_m(\rho)$, where G_m is the solution of (29).

Thus, there are two potential asymptotic blowup vortex profiles of the NLS, ψ_{R_m} and ψ_{G_m} .

In the case of non-vortex solutions ($m = 0$) there are also two blowup profiles, ψ_R and ψ_G . It is very easy to distinguish between these two blowup profiles numerically, since:

- (1) Solutions collapsing with ψ_R are peak-type solutions, i.e., the maximum of R is attained at $r = 0$, and they decrease monotonically for $0 \leq r < \infty$, whereas ψ_G solutions are ring-type solutions, i.e., they attain their global maximum at some $r_{\max} > 0$ and decreases monotonically away from r_{\max} .
- (2) The power collapsing into the singularity is $\approx P_{\text{cr}}$ for solutions collapsing with ψ_R , but significantly higher than P_{cr} for solutions collapsing with the ψ_G profile.

Unfortunately, one cannot use these characteristics to distinguish between ψ_{R_m} and ψ_{G_m} , since:

- (1) Both ψ_{R_m} and ψ_{G_m} are ring-type. Moreover, with a proper choice of f_c , the G_m profile can be extremely close to the R_m profile, see, e.g., Fig. 14.
- (2) Since G_m can be extremely close to R_m , collapse with ψ_{G_m} is possible at powers extremely close to $P_{\text{cr}}(m)$.

Therefore, we reach the conclusion that the best way to distinguish numerically between a ψ_{R_m} collapse and a ψ_{G_m} collapse is as follows. Recall that solutions collapsing with ψ_{R_m} have a faster-than-a-square-root blowup rate, while solutions that collapse with ψ_{G_m} have a square-root blowup rate. Therefore, following [8] we monitor LL_t , since $\lim_{t \rightarrow T_c} LL_t = -f_c^2/2$ goes to a zero in the first case but to a negative constant in the second case. In addition, when

$$f_c = \sqrt{-2 \lim_{t \rightarrow T_c} LL_t} > 0, \tag{60}$$

we can gain additional confidence that the solution indeed collapses with the ψ_{G_m} profile as follows. We search for the value of f_c for which G_m has the best match with the self-similar profile of the collapsing solution, and confirm that it agrees with the value of f_c obtained from the blowup rate using (60).

4.6.3. Simulations

We now present numerical investigations of collapsing critical vortex solutions, to see whether ψ_{G_m} and/or ψ_{R_m} are attractors. All the simulations presented in this section are for $m = 2$. We repeated these simulations for the cases of $m = 1$ and $m = 4$, and received similar results (data not shown).

We first solve Eq. (4) with the initial condition

$$\psi_0 = 1.02R_{m,0}(r)e^{im\theta}, \quad m = 2, \tag{61}$$

and observe that the numerical solution indeed collapses with a ring profile (see Fig. 15(A)). In order to check for self-similarity, in Fig. 15(B) we rescale the numerical solution according to

$$\psi_{\text{rescaled}} = \frac{1}{L(t)} \psi \left(\frac{r}{L(t)} \right), \quad L(t) = \frac{\max_r |\psi_0|}{\max_r |\psi|}. \tag{62}$$

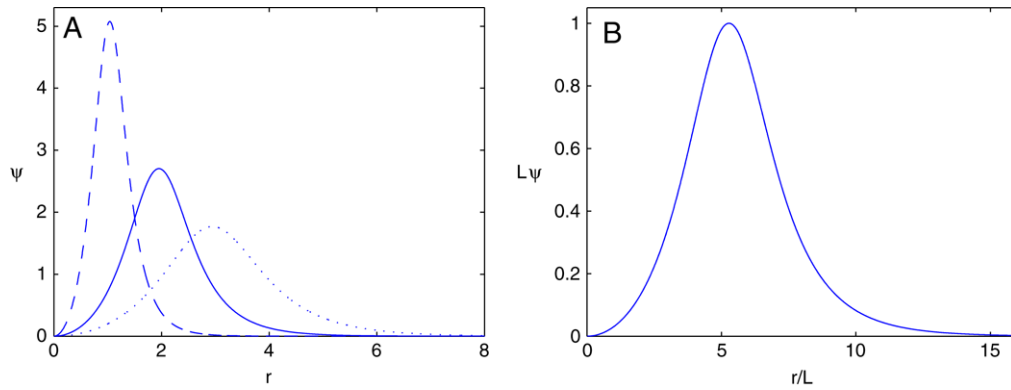


Fig. 15. A: Solution of (17) with initial condition (61) at $t = 0$ (dots, $L^{-1} = 1$), $t = 6.03$ (solid, $L^{-1} = 1.49$) and $t = 7.52$ (dashes, $L^{-1} = 2.8$). B: The second and third lines from A at focusing levels $L^{-1} = 1.49, 2.8$, normalized according to (62). Also plotted is the solution at the focusing level of $L^{-1} = 5.28 \times 10^{14}$ (dash-dots). All three lines are indistinguishable.

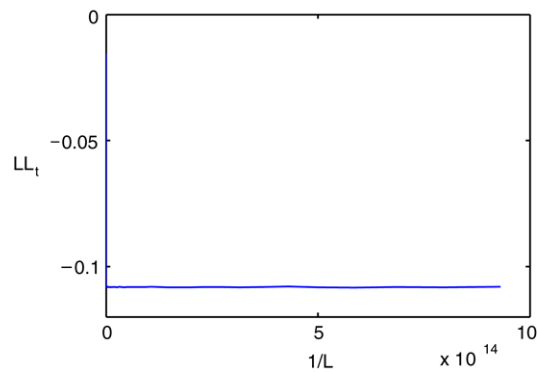


Fig. 16. LL_t as a function of focusing factor $1/L(t)$ for the solution of Fig. 15.

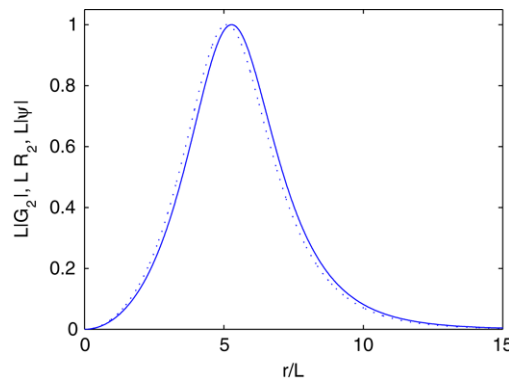


Fig. 17. A: Solid line: Self-similar profile from Fig. 15(B). Dashed line: $G_{2,0}(r)$ with $f_c = 0.4652$ and $g_0 = 0.14$. The two lines are indistinguishable. The dotted line is $R_{2,0}(r)$.

As expected, the normalized solution remains unchanged while focusing by a factor of 10^{14} , indicating that the solution indeed undergoes self-similar collapse.

In order to find the blowup rate of the solution, in Fig. 16 we plot LL_t as a function of $1/L$. Since $\lim_{t \rightarrow T_c} LL_t = -0.1092 < 0$, this indicates that $L \sim f_c \sqrt{T_c - t}$ with $f_c \approx \sqrt{-2 \cdot 0.1092} = 0.4673$, see Eq. (60). Therefore, Fig. 16 suggests that the solution that started with a perturbed $R_{2,0}$ profile collapsed the self-similar $G_{2,0}$ profile. To confirm that this is indeed the case, we search for the value of f_c that yields the $G_{2,0}$ profile that has the best fit to the self-similar profile of Fig. 15, and see that there is an excellent match between the two profiles, see Fig. 17. In contrast, the self-similar profile of the collapsing solution does not agree as well with $R_{2,0}(r)$. In addition, there is an excellent agreement, of less than 0.5% difference, between the value of $f_c = 0.4652$ of the best-fitting $G_{2,0}$ profile and the value of $f_c = 0.4673$ obtained from the blowup rate, see Eq. (60). Therefore, we conclude that *the perturbed $R_{2,0}$ vortex profile collapses with a self-similar $G_{2,0}$ profile at a square-root blowup rate.*

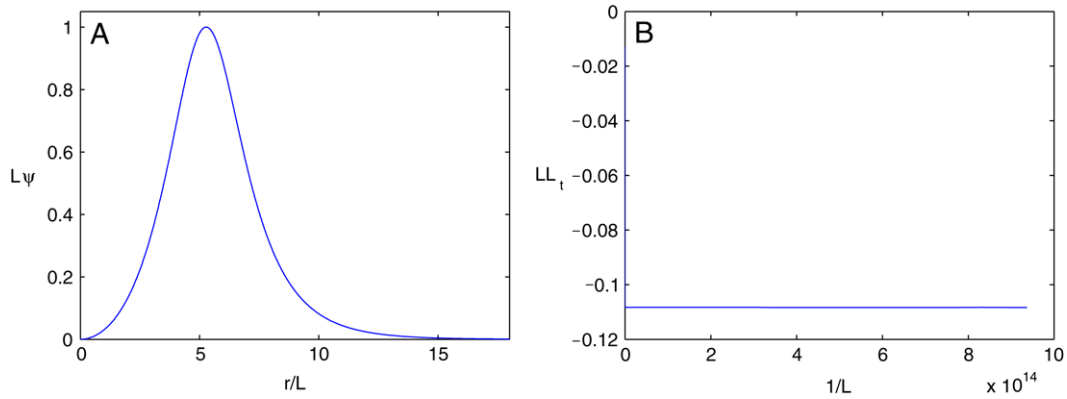


Fig. 18. Solution of (17) with initial condition (63). A: Solution rescaled according to (62), at $t = 0$ ($L^{-1}(t) = 1$, dots), at $t = 21.62$ ($L^{-1}(t) = 1.82$, solid), $t = 25.87$ ($L^{-1}(t) = 3.70 \times 10^7$, dash-dots), and at $L^{-1}(t) = 9.37 \times 10^{14}$, (time t differs only in the 14th digit, dashes). The four lines are indistinguishable. B: LL_t as a function of focusing factor $1/L(t)$.

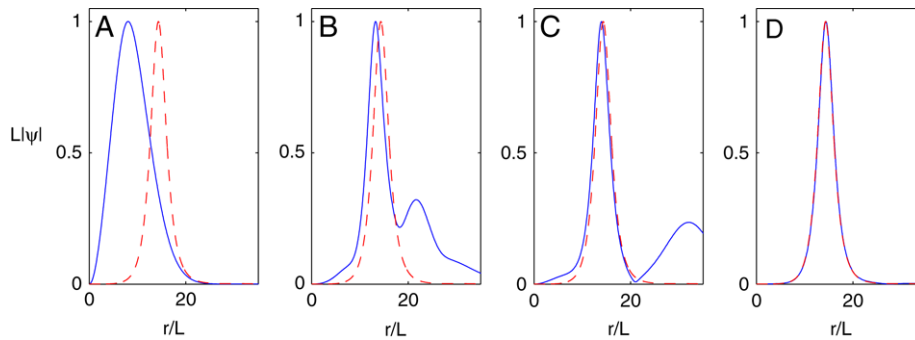


Fig. 19. Solution of the NLS (17) with the Laguerre-Gaussian initial condition $\psi_0 = \frac{1}{3}r^2e^{-(r/4)^2+i2\theta}$, rescaled according to (62). A: $t = 0$, $L^{-1}(t) = 1$; B: $t = 1.09$, $L^{-1}(t) = 3.76$; C: $t = 1.44$, $L^{-1}(t) = 5.30$; D: $t = 1.77$, $L^{-1}(t) = 26.3$. Dashed curve in A–D is the G_2 vortex profile with $f_c \approx 0.410$ and $g_0 = 5.07 \times 10^{-5}$.

We now study the collapse of the explicit blowup solution ψ_{G_m} . In order to construct the corresponding initial condition we first derive a simpler form of (30). To do so, we apply the dilation symmetry $\tilde{\psi} = \lambda\psi(\lambda^2t, \lambda r)$ with $\lambda = f_c\sqrt{T_c}$ to (30). Then at $t = 0$,

$$\psi_0 = G_{2,0}(r)e^{2i\theta - if_c^2r^2/8}. \quad (63)$$

We set $g_0 = 0.14$ and $f_c \approx 0.4652$ which corresponds to the $G_{2,0}$ profile of Fig. 17. Fig. 18(A) shows that the asymptotic self-similar profile is the same as the initial $G_{2,0}$ profile. In Fig. 18(B) we see that $\lim_{t \rightarrow T_c} LL_t = -0.1083$, indicating that $L \sim f_c\sqrt{T_c - t}$ with $f_c = 0.4654$, see (60), i.e., the blowup rate is a square root and the value of f_c has less than 0.05% difference with the value of f_c of the $G_{2,0}$ profile. Therefore, we conclude that the solution collapsed with the $\psi_{G_{2,0}}$ profile at a square-root blowup rate. This observation is not surprising since the solution $\psi_{G_{2,0}}$ is known analytically. However, the fact that the numerical solution maintained a self-similar profile while focusing over 15 orders of magnitude suggests that the self-similar single-ring $G_{2,0}$ profile is stable.

To see that $\psi_{G_{m,0}}$ is a strong attractor, we solve the NLS (4) with a Laguerre-Gaussian initial condition $\psi_0 = \frac{1}{3}r^2e^{-(r/4)^2+i2\theta}$ with $P = 4.12P_{cr}(2) \approx 31.6P_{cr}$. The G_2 profile which best fits the self-similar collapse profile is a $G_{2,0}$ profile with $f_c = 0.410$ and $g_0 = 5.07 \times 10^{-5}$, see Fig. 19. There is also an excellent agreement, of less than 0.3% difference, between the value of f_c of the best-fitting G_2 profile and the value of $f_c = 0.409$ obtained from the blowup rate.

As noted in Section 4.2.2, Eq. (29) also gives rise to the k -ring solutions $G_{m,k}$. We now show that $\psi_{G_{m,k}}$ k -ring solutions are highly unstable and evolve into a single-ring $\psi_{G_{m,0}}$ profile. To do so, we construct a $\psi_{G_{2,2}}$ initial condition (63) where we choose the parameters of the $G_{2,2}$ profile as $f_c = 0.35$ and $g_0 = 2.07 \times 10^{-5}$. In this case, the double-ring solution breaks and collapses with a single-ring solution. The $G_{2,0}$ profile which best fits the self-similar collapse profile is with $f_c = 0.367$ and $g_0 = 2.9 \times 10^{-6}$, see Fig. 20. There is also an excellent agreement, of approximately 0.05% difference, between the value $f_c = 0.3671$ of the best-fitting $G_{2,0}$ profile and the value $f_c = 0.3669$ obtained from the blowup rate. We note that in the simulation of Fig. 20 we use the same numerical parameters (grid resolution, etc.) as in the simulation in Fig. 18 which maintained the self-similar profile after focusing by a factor of 10^{15} . Therefore, this suggests that the single-ring solution $\psi_{G_{m,0}}$ is stable.

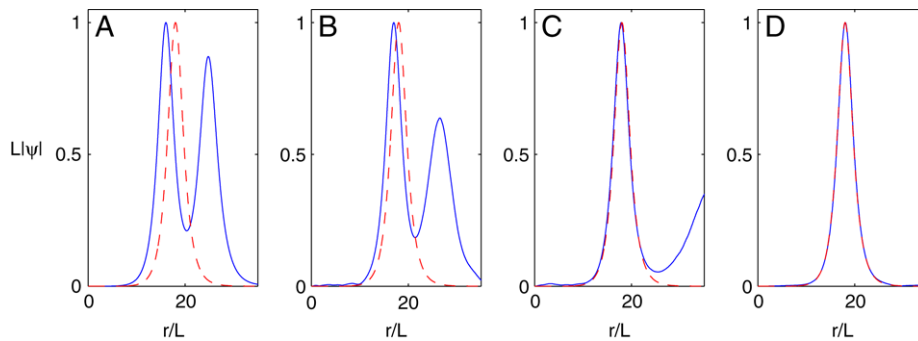


Fig. 20. Solution of (17) with the initial condition (63) with $m = 2$, $f_c = 0.35$ and $g_0 = 2.07 \times 10^{-5}$ rescaled according to (62), at A: $t = 0 (L^{-1}(t) = 1)$; B: $t = 27.04 (L^{-1}(t) = 3.39)$; C: $t = 27.60 (L^{-1}(t) = 7.19)$; D: $t = 27.81 (L^{-1}(t) = 36.10)$. The dashed line is the G_2 profile with $f_c = 0.367$ and $g_0 = 2.9 \times 10^{-6}$.

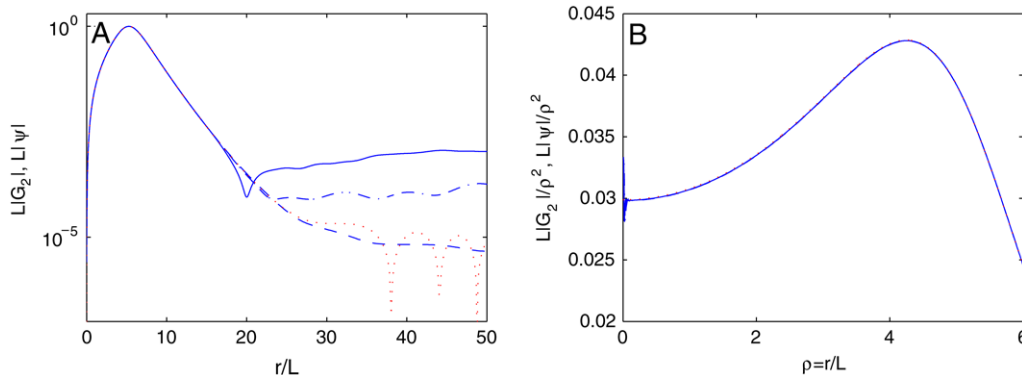


Fig. 21. A: Same data as in Fig. 15(B) on a semi-logarithmic scale. The dotted curve is the $G_{2,0}$ profile from Fig. 17. B: Plot of $L|\psi|/\rho^2$ where $\rho = r/L$ and ψ is the same solution as in A. The dotted curve is the $g_{2,0} = L G_{2,0}/\rho^2$ profile from Fig. 17. The four lines are indistinguishable.

4.6.4. Quasi-self-similar collapse

The simulations of Section 4.6.3 suggest that “all” vortex solutions of the NLS undergo a self-similar collapse with the singlering ψ_{G_m} profile. In fact, the blowup profile is “only” quasi-self-similar, i.e.,

$$\psi \sim \begin{cases} \psi_{G_m} & 0 \leq r/L \ll \rho_0 \\ \psi_{\text{outer}} & \rho_0 \ll r/L, \end{cases} \tag{64}$$

where $\rho_0 \gg 1$ is a constant that depends on the initial condition and $L(t) = \|\psi(t, r, \theta)\|_1^{-1}$. To see that, in Fig. 21(A) we plot the same data as in Fig. 15(B) on a semi-logarithmic scale. It can be seen that the NLS solution rescaled according to (62), remains unchanged in the region $0 \leq r/L \leq 15$ while focusing by a factor of 10^{15} , but varies in the region $r/L > 20$. Hence, the solution does not undergo self-similar collapse, but “only” quasi-self-similar collapse. In addition, the best-matching $G_{m,0}$ profile (taken from Fig. 17) has an excellent match with the rescaled NLS solution in the region $0 \leq r/L < 15$, but not in the region $r/L > 20$.

We note that quasi-self-similar collapse is consistent with Theorem 23 that all singular NLS solutions converge to a self-similar profile. To see that, we provide the following informal argument. Assume that the solution undergoes a quasi-self-similar collapse of the form (64). Since, near the collapse point ψ_{outer} is frozen in time, $\psi_{\text{outer}}(t, r) \approx f(r)$ as $t \rightarrow T_c$. Therefore, $S(\psi)$ is given by, see (59), $S(\psi)(r, t) = \begin{cases} G_m(r) & 0 \leq r \ll r_0 \\ Lf(Lr) & r_0 \ll r. \end{cases}$

Therefore, $S(\psi)(r, t) \xrightarrow{L^p} \Psi(r)$ for $p > 2$, where $\Psi = \begin{cases} G_m(r) & 0 \leq r \ll r_0 \\ 0 & r_0 \ll r. \end{cases}$

Recall that non-vortex NLS ring solutions that blowup with $\psi_{G_{0,0}}$ also undergo quasi-self-similar collapse, see Fig. 22. In that case, ψ_G characterizes only the collapsing ring region, and not the inner region $r/L = \mathcal{O}(1)$ or the outer region $r/L \gg \rho_0$, i.e.,

$$\psi \sim \begin{cases} \psi_{\text{inner}} & 0 \leq r/L \ll \rho_0 \\ \psi_{G_{0,0}} & \rho_0 \ll r/L \ll \rho_1 \\ \psi_{\text{outer}} & \rho_1 \ll r/L. \end{cases} \tag{65}$$

Thus, unlike the non-vortex singular rings, the singular vortex solution is self-similar with the $G_{m,0}$ profile also in the inner region $r/L = \mathcal{O}(1)$. We already saw this in Fig. 21(A). However, since for vortex solutions $|\psi| \sim r^m$ near the origin, the plot of ψ near $r = 0$ may be misleading in determining self-similarity. Therefore, to better verify that the NLS vortex solution is self-similar for

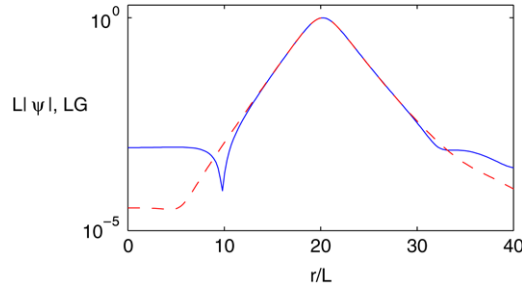


Fig. 22. Non-vortex collapsing ring solution of the NLS (solid) and the best-fitted G profile (dashes) normalized according to (62). From [8, Figure 15E].

$r/L = \mathcal{O}(1)$, we plot $|\psi|/r^m$, rescaled according to (62), in Fig. 21(B), and observe that it remains unchanged in the inner region $r/L = \mathcal{O}(1)$, and has an excellent match with the self-similar profile $g_{2,0} = G_{2,0}/r^2$. Therefore, we conclude that, indeed, the singular vortex solution is also self-similar in the inner region $r/L = \mathcal{O}(1)$.

4.6.5. Summary: Radially-symmetric case

In Section 4.6 we studied numerically the collapse behavior of four different vortex solutions that were initially either close to the $\psi_{G_{m,0}}$ profile or to the $\psi_{R_{m,0}}$ profile, or far from both profiles. In all cases, the solutions collapsed with the $\psi_{G_{m,0}}$ profile at a square-root blowup rate. *These simulations suggest that $\psi_{G_{m,0}}$ is a strong attractor for m -vortex solutions of the critical NLS, while $\psi_{R_{m,0}}$ is unstable.*

The $\psi_{G_{m,0}}$ solutions, however, have an infinite power (L^2 norm), see Lemma 8. This seems to suggest that $\psi_{G_{m,0}}$ cannot be the asymptotic profile of H^1 vortex solutions of the critical NLS. However, in Section 4.6.4 we saw that the collapsing solution is only quasi-self-similar, and that the self-similar profile $\psi_{G_{m,0}}$ characterizes only the collapsing ring region and not the whole solution. Therefore, the infinite-power tail of the vortex profile $G_{m,0}$ may be “irrelevant” to the NLS ring solutions, as can be seen in Fig. 21.

A similar situation appears in the vortex-free case $m = 0$ [8], where $\psi_{G_{0,0}}$ characterizes only the collapsing ring region and not the whole solution, see (65), so that the infinite-power tail of ψ_G is also “irrelevant”. The numerical simulations in [8] show that H^1 ring solutions of the NLS collapse with an asymptotic quasi-self-similar blowup profile $\psi_{G_{0,0}}$ up to focusing levels of 10^{16} . However, it is impossible to determine numerically whether these solutions maintain a ring profile all the way until the singularity or whether at some exceedingly large focusing factor the ring structure breaks up and they collapse with the $\psi_{R_{0,0}}$ profile. It is therefore an open question whether there exist H^1 non-vortex solutions of the NLS that collapse with the self-similar ring profile $\psi_{G_{0,0}}$ at a square-root rate.

The surprising observation that the finite-power vortex solutions which start close to $\psi_{R_{m,0}}$ collapse as $\psi_{G_{m,0}}$ suggests that $\psi_{G_{m,0}}$ may, indeed, be the asymptotic quasi-self-similar profile of H^1 vortex solutions of the critical NLS all the way up to the singularity. However, as in the vortex-free case, at present, whether this is indeed the case is an open question.

4.6.6. Azimuthal instability of collapsing vortex solutions

The simulations of Section 4.6.3 suggest that the self-similar profile $\psi_{G_{m,0}}$ is a strong attractor in the radially-symmetric case, i.e., when $\psi_0 = e^{im\theta} A_0(r)$. We now test its stability in the anisotropic case, i.e., under symmetry-breaking perturbations. To do that, we modify the method which was developed by Soto-Crespo and co-workers in [9,10] for azimuthal modulation instability of stationary vortex-free ring solutions. This method was later applied to stationary vortex solutions [29,5]. To the best of our knowledge, this (or any other) method has not been used to analyze the azimuthal modulation stability of *collapsing* rings or vortices. To do that, we consider a perturbed collapsing $\psi_{G_{m,0}}$ of the form⁸

$$\psi = \psi_{G_{m,0}} \left(1 + \mu \cos(\Omega\theta) e^{\delta_\Omega \tau} + \mathcal{O}(\mu^2) \right), \quad \mu = \mu_r + i\mu_i, \tag{66}$$

where $\tau = \int_0^t \frac{ds}{L^2(s)}$, Ω is the number of filaments (modulations) and δ_Ω is the growth rate of the filaments.

Linear stability analysis gives (see Appendix G),

$$\delta_\Omega(\rho) = \left(\frac{\Omega}{\rho} \right) \sqrt{2G_{m,0}^2(\rho) - \left(\frac{\Omega}{\rho} \right)^2}. \tag{67}$$

For $0 \leq \Omega \leq \sqrt{2\rho}G_{m,0}$ the growth rate δ_Ω is positive, therefore the solution is unstable. The fastest-growing mode is the one for which δ_Ω is the largest, and is given by

$$\Omega = G_{m,0}(\rho) \cdot \rho. \tag{68}$$

⁸ For comparison, the ansatz used in [9] for stationary rings is $\psi = \psi_G^{\text{stationary}} + \mu \cos(\Omega\theta) e^{\delta_\Omega t} + \mathcal{O}(\mu^2)$.

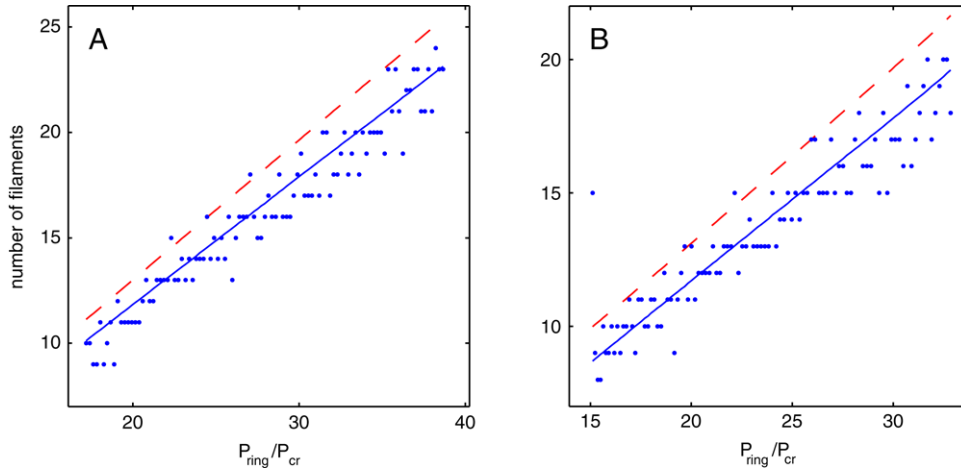


Fig. 23. Number of filaments (Ω) as a function of vortex initial power P_{ring} , see Eq. (33). The dashed curve is Ω_{max} , the solid curve is Ω_{mean} . A: $m = 2$, $\Omega_{\text{max}} \approx 0.66 \frac{P}{P_{\text{cr}}} - 0.25$ and $\Omega_{\text{mean}} \approx 0.6 \frac{P}{P_{\text{cr}}} - 0.26$. B: $m = 4$, $\Omega_{\text{max}} \approx 0.65 \frac{P}{P_{\text{cr}}} + 0.03$ and $\Omega_{\text{mean}} \approx 0.61 \frac{P}{P_{\text{cr}}} - 0.52$.

We now discuss how to choose ρ so that Eq. (68) predicts the number of filaments. One option is to choose ρ that maximizes the value of Ω , i.e.,

$$\Omega_{\text{max}} = \max_{\rho} G_{m,0}(\rho) \cdot \rho. \quad (69)$$

In this case, $\rho \approx \rho_{\text{max}}$ where ρ_{max} is the location of the vortex peak. The choice (69) can be expected to give an upper-bound estimate. Another option, used in [9,10], is to take the mean value of Ω over the vortex peak region. For example, we can use

$$\Omega_{\text{mean}} = \frac{\int_{\rho_{\text{max}}-1}^{\rho_{\text{max}}+1} \Omega(\rho) |\psi_{G_{m,0}}(\rho)|^2 \rho d\rho}{\int_{\rho_{\text{max}}-1}^{\rho_{\text{max}}+1} |\psi_{G_{m,0}}(\rho)|^2 \rho d\rho}. \quad (70)$$

To test the validity of the predictions (69) and (70) for the number of filaments, we choose one-hundred different $G_{m,0}$ profiles with g_0 ranging from $g_0 = 10^{-8}$ to $g_0 = 6 \times 10^{-4}$. Recall, that as g_0 decreases, the vortex radius, hence, its power increases (see Section 4.2.2). For each $G_{m,0}$ we solve the NLS with an initial condition that is a perturbed $\psi_{G_{m,0}}^{\text{explicit}}$ at $t = 0$, i.e., $\psi_0 = (1 + \varepsilon_1(\mathbf{x})e^{i\varepsilon_2(\mathbf{x})})\psi_{G_{m,0}}^{\text{explicit}}(0)$, where $\varepsilon_1(\mathbf{x})$ and $\varepsilon_2(\mathbf{x})$ are random functions which depend on (x, y) , hence are symmetry breaking. We run this series of one-hundred simulations for $m = 2$ and for $m = 4$. Typically, after focusing by a factor of 1.5, the vortex ring breaks into several filaments. In Fig. 23 we plot the number of filaments for each simulation. As expected, Ω_{max} is an upper limit for the number of filaments, whereas Ω_{mean} provides a good estimate to the average number of filaments.

Azimuthal modulation instability of vortices was also analyzed in [29,5]. The number of filaments predicted in these studies is different from our prediction, yet was in agreement with the numerical simulations conducted in these studies. The reason for this difference in the number of filaments is that these studies considered initial conditions far from ψ_G with high noise level. The noise caused the vortex to break into filaments before it could start to collapse and approach the ψ_G profile. Therefore, the analysis in [29, 5] predicts the number of filaments for essentially stationary vortices. In contrast, we study a different regime where the initial noise is small enough to allow the vortex solution to collapse with ψ_G profile and only then breakup.

5. Singular vortices of the supercritical NLS

5.1. Asymptotic blowup profiles in the vortex-free case

We now briefly review the theory of asymptotic blowup profiles of the d -dimensional supercritical NLS

$$i\psi_t(t, r) + \psi_{rr} + \frac{d-1}{r}\psi_r + |\psi|^{2\sigma}\psi = 0, \quad \sigma d > 2, \quad (71)$$

in the vortex-free case. Until recently, it was believed that “all” singular solutions of the supercritical NLS (71) collapse with a quasi-self-similar peak profile ψ_S , i.e., $\psi(t, r) \sim \psi_S(t, r)$, where

$$\psi_S(t, r) = \frac{1}{L^{1/\sigma}(t)} S(\rho) e^{i\tau + i\frac{L}{4t}r^2}, \quad \tau = \int_0^t \frac{ds}{L^2(s)}, \quad \rho = \frac{r}{L(t)},$$

and S is the “peak-type” solution of

$$S_{\rho\rho} + \frac{d-1}{\rho} S_{\rho} + \left(\frac{f_c^2}{16} \rho^2 - 1 - i \frac{f_c(\sigma d - 2)}{4} \right) S + |S|^{2\sigma} S = 0, \quad S'(0) = 0, \quad S(\infty) = 0.$$

These solutions have a square-root blowup rate, i.e., $L(t) \sim f_c \sqrt{T_c - t}$ where f_c is a positive constant whose value depends on the initial condition.

In 2006, Raphael [30] proved the existence and stability of a new type of singular solutions of the quintic two-dimensional NLS (i.e., $\sigma = 2, d = 2$) that have a self-similar ring profile. Surprisingly, the ring radius approaches a positive constant as these solutions collapse. Hence, these solutions blow up on a curve, and not at a point. The blowup rate of these “standing ring” solutions is a square root with a loglog correction.

In [11], we showed that the critical non-vortex ring solution ψ_G , see [8] and Section 4.6, and Raphael’s standing ring solutions belong to a two-parameter family of ring solutions of the d -dimensional NLS

$$i\psi_t(t, r) + \psi_{rr} + \frac{d-1}{r} \psi_r + |\psi|^{2\sigma} \psi = 0, \quad 2/d \leq \sigma \leq 2, \quad 1 < d. \tag{72}$$

These solutions collapse with a quasi-self-similar ring profile ψ_Q , i.e., $\psi \sim \psi_Q$ where

$$\psi_Q = \frac{1}{L^{1/\sigma}(t)} Q(\rho) e^{i\tau + i\alpha \frac{L^2}{4L} r^2 + i(1-\alpha) \frac{L^2}{4L} (r-r_{\max}(t))^2}, \tag{73}$$

and $\tau = \int_0^t \frac{ds}{L^2(s)}$, $\rho = \frac{r-r_{\max}(t)}{L}$ and $r_{\max}(t) = r_0 L^\alpha(t)$. Here, $r_{\max}(t)$ is the ring radius, i.e., the location of the ring peak, and $L(t)$ is the ring width, see Fig. 9. The value of the parameter α , which defines the relation between the ring radius $r_{\max}(t)$ and the ring width $L(t)$, turned out to be given by $\alpha = \frac{2-\sigma}{\sigma(d-1)}$.

In the supercritical case, the self-similar Q profile is given by

$$Q = \omega^{\frac{1}{\sigma}} (1 + \sigma)^{\frac{1}{2\sigma}} [\operatorname{sech}(\omega\sigma\rho)]^{\frac{1}{\sigma}}, \quad \omega = \sqrt{1 - \frac{\alpha r_0^2}{4(1+\alpha)^2} f_c^{2(1+\alpha)}}, \tag{74}$$

and in the critical case, the self-similar Q profile is the single-ring solution of the G equation [8].

The asymptotic profile ψ_Q has two radial phase terms. The quadratic phase term centered at $r = 0$ corresponds to focusing towards the origin, and the quadratic phase term centered at $r = r_{\max}(t)$ corresponds to focusing towards $r_{\max}(t)$. The blowup behavior of ψ_Q is, therefore, a combination of “global” ring focusing towards the origin, together with ring width shrinking towards $r_{\max}(t)$. The ratio between the two phase terms is determined by the parameter α .

It is useful to distinguish the following three cases:

- (1) $\alpha = 1$ ($\sigma d = 2$, **critical NLS**): In this case, the quadratic phase term centered at $r = r_{\max}(t)$ vanishes. Since $r_{\max}(t) = r_0 L$, this case was denoted in [11] as *equal-rate collapse*. In this case, ψ_Q is given by ψ_G .
- (2) $\alpha = 0$ ($\sigma = 2$, **quintic NLS**): In this case, the “global” ring focusing phase term disappears. Since $r_{\max}(t) \equiv r_0$, this case describes a collapsing *standing ring solution*. In the two-dimensional case, ψ_Q is exactly Raphael’s standing ring solution.
- (3) $0 < \alpha < 1$ ($2/d < \sigma < 2$): In this case, both phase terms affect the blowup dynamics. Since $r_{\max}(t) = r_0 L^\alpha$, the ring radius shrinks to zero, but at a slower rate than the ring width L .

The blowup rate of ψ_Q is given by

$$L(t) \sim \begin{cases} f_c (T_c - t)^{\frac{1}{1+\alpha}}, & \frac{2}{d} \leq \sigma < 2, \quad (0 < \alpha \leq 1), \\ \sqrt{\frac{2\pi(T_c - t)}{\log \log \frac{1}{T_c - t}}}, & \sigma = 2, \quad (\alpha = 0) \end{cases} \tag{75}$$

where the constant f_c is the same as in (74). Hence, the NLS (72) can have singular ring-solutions with any blowup rate p , such that $1/2 \leq p < 1$.

5.2. Asymptotic profile of collapsing vortex solutions of the supercritical NLS

We now want to find the asymptotic profiles of collapsing vortex solutions of the two-dimensional supercritical NLS

$$i\psi_t(t, r) + \psi_{rr} + \frac{1}{r} \psi_r + |\psi|^{2\sigma} \psi = 0, \quad 1 < \sigma \leq 2. \tag{76}$$

As noted, in the vortex-free case, there are two asymptotic blowup profiles:

- (1) A peak-type solution ψ_S , which undergoes equal-rate collapse at a square-root blowup rate.
- (2) A ring-type solution ψ_Q , in which the ring radius shrinks to zero at a slower rate than the ring width, and collapses at a $\frac{1}{1+\alpha} = \sigma/2$ blowup rate.

We now show that this is also the same for $m > 0$, namely, there are two potential asymptotic blowup profiles:

- (1) ψ_{S_m} which undergoes equal-rate collapse at a square-root blowup rate.
- (2) ψ_{Q_m} , in which the ring radius shrinks to zero at a slower rate than the ring width, and collapses at a $\frac{1}{1+\alpha} = \sigma/2$ blowup rate.

Unlike the vortex-free case, however, both solutions are ring-type.

5.2.1. Square-root blowup rate (ψ_{S_m})

Let us consider vortex solutions of (71) that have the asymptotic form $\psi(t, r) \sim \psi_{S_m}(t, r)$, where

$$\psi_{S_m}(t, r) = \frac{1}{L^{1/\sigma}(t)} S_m(\rho) e^{i\tau + im\theta + i\frac{L_t}{4L}r^2}, \quad \tau = \int_0^t \frac{ds}{L^2(s)}, \quad \rho = \frac{r}{L(t)}, \tag{77}$$

and $L(t) \sim f_c \sqrt{T_c - t}$. Then, S_m is the solution of

$$S_m''(\rho) + \frac{1}{\rho} S_m' + \left(\frac{f_c^2}{16} \rho^2 - 1 - \frac{m^2}{\rho^2} - i \frac{f_c(\sigma - 1)}{2} \right) S_m + |S_m|^{2\sigma} S_m = 0, \tag{78}$$

$$S'(0) = 0, \quad S(\infty) = 0.$$

Lemma 25. Let $S_m(\rho)$ be a solution of (77). Then $S_m(\rho) = \rho^m s_m(\rho)$, where $s_0 = s_m(0) \neq 0$ and $s_m(\rho)$ is the analytic solution of

$$s_m''(\rho) + \frac{2m + 1}{\rho} s_m' - \left(1 - \frac{f_c^4}{16} \rho^2 - i \frac{f_c(\sigma - 1)}{2} \right) s_m + \rho^{2m\sigma} |s_m|^{2\sigma} s_m = 0, \quad s_m'(0) = 0, \quad s_m(\infty) = 0. \tag{79}$$

Proof. The proof of Lemma 25 is identical to the proof of Lemma 3 in Appendix B. \square

5.2.2. $\sigma/2$ blowup rate (ψ_{Q_m})

We now show that the asymptotic profile ψ_Q from (73), multiplied by $e^{im\theta}$, is an asymptotic profile for vortex solutions of the supercritical two-dimensional NLS (76) with initial condition $\psi_0 = e^{im\theta} A_0(r)$.

Proposition 26. Eq. (76) has singular vortex solutions whose asymptotic profile is given by $\psi_{Q_m} = \psi_Q \cdot e^{im\theta}$, where ψ_Q is given by (73). In addition,

(1)

$$\alpha = \frac{2 - \sigma}{\sigma}. \tag{80}$$

(2) The blowup rate is given by

$$L(t) \sim \begin{cases} (T_c - t)^{\frac{\sigma}{2}}, & 1 < \sigma < 2, \quad (0 < \alpha < 1), \\ \sqrt{\frac{2\pi(T_c - t)}{\log \log \frac{1}{T_c - t}}}, & \sigma = 2, \quad (\alpha = 0). \end{cases} \tag{81}$$

Proof. We follow the analysis in [11, Section 4]. Substitution of $\psi_Q \cdot e^{im\theta}$ into (76) gives

$$Q_{\rho\rho} + (d - 1) \frac{L}{L\rho + r_0 L^\alpha} Q_\rho - \left(1 + m^2 \left(\frac{L}{L\rho + r_0 L^\alpha} \right)^2 \right) Q + |Q|^{2\sigma} Q + A Q + i D Q = 0, \tag{82a}$$

where

$$A = -\frac{1}{4} \left[(L^3 \rho^2 + 2\alpha r_0 L^{2+\alpha} \rho + \alpha r_0^2 L^{1+2\alpha}) L_{tt} - \alpha(1 - \alpha) r_0 (r_0 L^{2\alpha} + 2L^{\alpha+1} \rho) L_t^2 \right],$$

$$D = \frac{d - 1}{2} \left[\alpha - \frac{2 - \sigma}{\sigma(d - 1)} + (1 - \alpha) \frac{L\rho}{L\rho + r_0 L^\alpha} \right] L L_t. \tag{82b}$$

As in [11], the admissible values of α are $0 \leq \alpha < 1$. Hence, $\varepsilon(t) = L^{1-\alpha}$ goes to zero as the solution approaches the singularity. Therefore, the phase term $e^{im\theta}$ contributes only to $\mathcal{O}(\varepsilon^2(t))$ terms. In [11], we saw that the blow profile, blowup rate, the relation between $r_{\max}(t)$ and $L(t)$ and the value of α are determined only by the $\mathcal{O}(1)$ and $\mathcal{O}(\varepsilon)$ terms of (82). Hence, all the results follow directly from the analysis in [11, Section 4]. \square

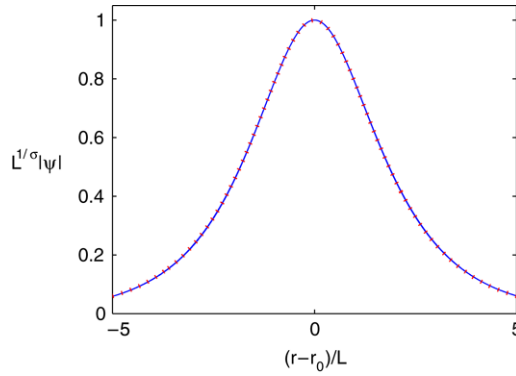


Fig. 24. Solution of (76) with $\sigma = 1.1$ for the initial condition (83) at $t = 0$ ($L^{-1} = 1$) (dashes); $t = 0.125$ ($L^{-1} \approx 1.18 \times 10^6$) (dash-dots) and ($L^{-1} \approx 1.74 \times 10^{11}$) (solid, time t differs from previous time only in the 14th digit). The dotted curve is $2\sqrt{1+\sigma} \operatorname{sech}^{1/\sigma}(\sigma r)$.

Remark 27. Note that the profile Q of ψ_{Q_m} is independent of m .

Remark 28. Proposition 26 can be extended to the critical case $\sigma = 1$ ($\alpha = 1$) as follows. Relation (80) for the value of α and relation (81) for the blowup rate remain unchanged, but the blowup profile is G_m , rather than Q , see Section 4.6.

Remark 29. We note that, as in [11], the derivation of the results in Proposition 26 is based on several assumptions and conjectures which are yet to be made rigorous. In particular, we can only show that the blowup rate is equal to or faster than $(T_c - t)^{\frac{1}{1+\alpha}}$ for $1 < \sigma < 2$ and equal to or faster than $(T_c - t)^{\frac{1}{2}}$ for $\sigma = 2$. However, the numerical simulations in Section 5.3 strongly suggest that the blowup rate is, indeed, given by (81).

5.3. Numerical study

We now present numerical investigations of collapsing supercritical vortex solutions, to see whether ψ_{Q_m} and/or ψ_{S_m} are attractors. All the simulations presented in this section are for $m = 2$.

5.3.1. Collapsing ψ_{Q_m} solutions

We consider the two cases $0 < \alpha < 1$ (Section 5.3.1.1) and $\alpha = 0$ Section 5.3.1.2). We use the initial condition $\psi_0 = \psi_Q^0 \cdot e^{im\theta}$ with $L(0) = \frac{1}{2^\sigma}$, $\frac{L_t(0)}{L(0)} = -4$, $r_0 L^\alpha(0) = 5$, and $\omega = 1$, to obtain, see Eq. (73),

$$\psi_0 = 2(1 + \sigma)^{1/2\sigma} [\operatorname{sech}(2^\sigma \sigma (r - 5))]^{1/\sigma} e^{-i\alpha r^2 - i(1-\alpha)(r-5)^2} e^{im\theta}. \tag{83}$$

The choice $L(0) = \frac{1}{2^\sigma}$ gives an initial condition which is sufficiently localized, so as to prevent a possible truncation of the sech ring tail near the origin.

5.3.1.1. *The case $0 < \alpha < 1$.* We first present a simulation with $\sigma = 1.1$. The expected value of α in this case is

$$\alpha = \frac{2 - 1.1}{1.1} = \frac{9}{11} \approx 0.8181, \tag{84}$$

see Eq. (80). In order to check for self-similarity, in Fig. 24 we rescale the numerical solution according to

$$\psi_{\text{rescaled}} = L^{1/\sigma} \psi \left(\frac{r - r_{\max}(t)}{L} \right), \quad L = \frac{\max_r |\psi_0|^\sigma}{\max_r |\psi|^\sigma}, \quad r_{\max}(t) = \operatorname{argmax}_r |\psi|. \tag{85}$$

As expected, the normalized solution remains unchanged while focusing by a factor of 10^{13} , indicating that the solution indeed undergoes self-similar collapse. In addition, the self-similar profile has an excellent agreement with the Q profile. Next, we calculate the parameter α of the ring radius shrinkage. According to Eq. (73), $r_{\max}(t) = r_0 L^\alpha$ where $\alpha \approx 0.8181$, see Eq. (84). To find the parameter α numerically, we calculate $r_{\max}(t)$ from Eq. (85) and plot $r_{\max}(t)$ as a function of $1/L$. Fig. 25(A) shows that $r_{\max}(t) \approx 9.672 L^\alpha$ with $\alpha = 0.81919$, which differs from the predicted value of α by about 0.12%. We now consider the *blowup rate* of these solutions. The expected blowup rate is $(T_c - t)^{\frac{\sigma}{2}}$, see Eq. (81). To find the blowup numerically we first plot the blowup rate L as a function of $T_c - t$ and find the best-fitting exponent p for $L \sim f_c(T_c - t)^p$. The results in Fig. 25(B) show that $L \sim f_c(T_c - t)^{0.549}$, perfectly fitting the expected value of $\frac{\sigma}{2} = 0.55$ with a relative error of less than 0.18%. Since plotting L as a function of $T_c - t$ is not sensitive enough to tell a $\frac{1}{1+\alpha}$ blowup rate from a slightly-faster-than-a $\frac{1}{1+\alpha}$ blowup rate, we plot $L^\alpha L_t$

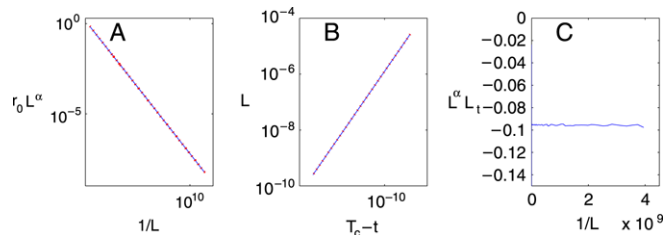


Fig. 25. Solution of Fig. 24. A: $r_{\max}(t)$ as a function of L . The dotted curve is the fitted curve $cL(t)^{0.81919}$ where $c = 9.672$. B: L as a function of $T_c - t$ on a logarithmic scale. The dotted curve is the fitted curve $L = c(T_c - t)^{0.549}$ where $c = 0.399$. C: $L^\alpha L_t$ as a function of $1/L$.

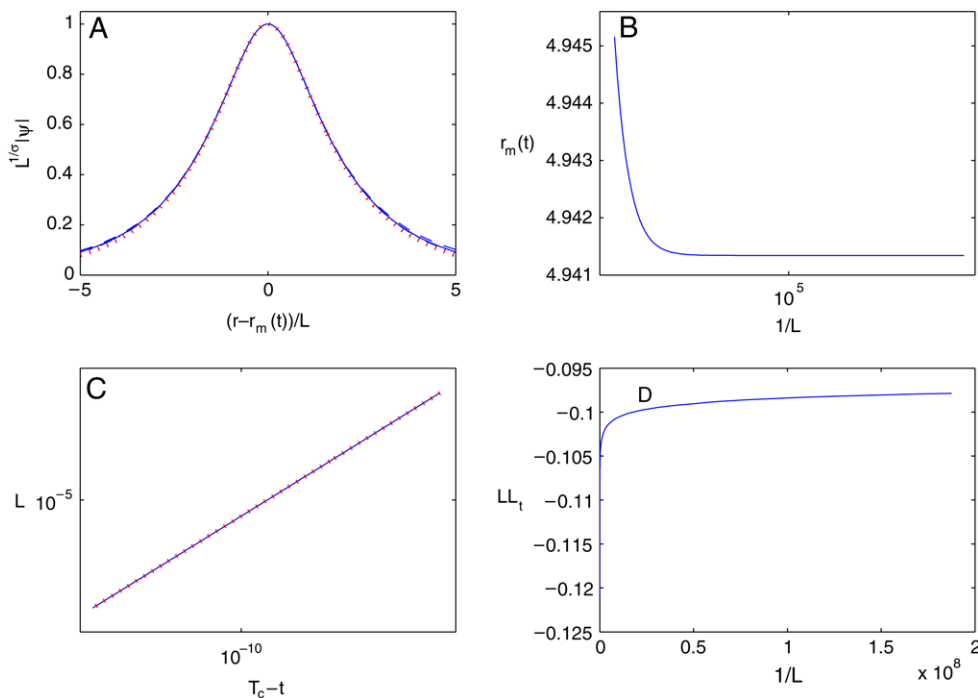


Fig. 26. Solution of quintic NLS ($\sigma = 2$) with ψ_0 given by (83) for $m = 4$ at A: Solution rescaled according to (85) at $t = 0$ ($L^{-1} = 1$, $r_{\max}(t) = 4.951$, dashed), $t = 0.0932$ ($L^{-1} = 4.44 \times 10^5$, $r_{\max}(t) = 4.941$, solid) and for $L^{-1} = 2.11 \times 10^9$ (dash-dotted). Values of t and $r_{\max}(t)$ differ only in the 10th digit or after, therefore only the focusing level is quoted. The bold dotted curve is $P = \text{sech}^{\frac{1}{2}}(2\sqrt{3}(r - 5))$ B: Ring radius as a function of focusing factor $1/L$. C: L as a function of $T_c - t$. The dotted curve is the fitted curve $c(T_c - t)^{0.50372}$. D: LL_t as a function of the focusing factor $1/L$.

as a function of the focusing factor $1/L$. For a blowup rate equal to $\frac{1}{1+\alpha}$, $L^\alpha L_t$ goes to a negative constant, but for a blowup rate faster than $\frac{1}{1+\alpha}$, $L^\alpha L_t$ goes to zero. The results in Fig. 25(C) show that $\lim_{t \rightarrow T_c} L^\alpha L_t = -0.0951$, indicating that the blowup rate is equal to $(T_c - t)^{\frac{\sigma}{2}}$.

5.3.1.2. The case $\alpha = 0$. We now study collapsing vortex solutions in the case of the quintic two-dimensional NLS ($\sigma = 2$) with the initial condition (83). The expected value of α in this case is $\alpha = \frac{2-2}{2} = 0$, see Eq. (80).

In order to check for self-similarity we rescale the solution ψ according to (85). Fig. 26(A) shows that all rescaled plots of the solution at focusing levels varying from 10^1 to 10^8 are nearly indistinguishable, indicating that the solution is indeed self-similar while focusing over 6 orders of magnitude. In addition, Fig. 26(A) also shows that the rescaled profile perfectly fits the Q profile. In Fig. 26(B) we plot $r_{\max}(t)$ as a function of the focusing factor $1/L$. It can be seen that $\lim_{t \rightarrow T_c} r_{\max}(t) \cong 4.944$, i.e., the ring is standing and not shrinking towards the origin. Next, we consider the blowup rate of the standing ring solution. To do so, we first assume that $L \sim f_c(T_c - t)^p$ and find the best-fitting p . Fig. 26(C) shows that $p \approx 0.50372$, indicating that the blowup rate is square root or slightly faster. Next, we check whether L is slightly faster than a square root, by plotting LL_t as a function of the focusing factor $1/L$. Recall that for a square-root blowup rate, LL_t will go to a negative constant as $t \rightarrow T_c$, while for a faster-than-a-square-root blowup rate LL_t goes to zero [8]. The results in Fig. 26(D) show that $\lim_{t \rightarrow T_c} LL_t = 0$, indicating that the blowup rate is faster-than-a-square-root, in agreement with (81).

5.3.1.3. Shrinkage and blowup rates. Relation (80) for the shrinkage rate parameter α and relation (81) for the blowup rate were found to be in excellent agreement for the two simulations presented so far in this section. We now systematically verify the

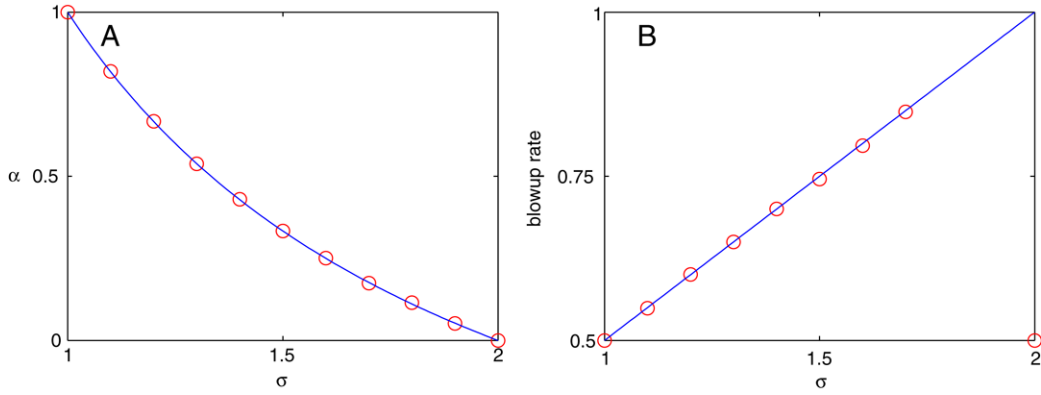


Fig. 27. A: Computed values of the shrinkage rate parameter α (circles). The solid curve is Eq. (80). B: Computed blowup rate (circles). The solid curve is $\frac{1}{1+\alpha} = \frac{\sigma}{2}$.

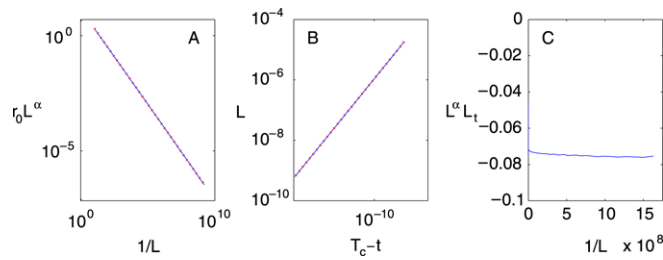


Fig. 28. Solution of Fig. 24. A: $r_{\max}(t)$ as a function of L . The dotted curve is the fitted curve $cL(t)^{0.823}$ where $c = 13.47$. B: L as a function of $T_c - t$ on a logarithmic scale. The dotted curve is the fitted curve $L = c(T_c - t)^{0.547}$ where $c = 0.327$. C: $L^\alpha L_t$ as a function of $1/L$.

validity of these relations. Fig. 27(A) shows that for $\sigma = 1, 1.1, 1.2, \dots, 2$, the difference between the numerical value of the best-fitting α in $r_{\max} \approx r_0 L^\alpha$ and the analytic prediction (80) is less than 3%. In Fig. 27(B) we plot the blowup rates measured. For $\sigma = 1, 1.1, 1.2, \dots, 1.7$ the blowup rate is $f_c(T_c - t)^p$, where the difference between p and $\frac{1}{1+\alpha}$ is less than 2%. In addition, in all these simulations, $L^\alpha L_t \rightarrow \text{Const} \neq 0$ (data not shown), showing that the blowup rate is $\frac{1}{1+\alpha} = \frac{\sigma}{2}$ with no loglog-type corrections. When $\sigma = 2$, $p = 0.5001$ and $LL_t \rightarrow 0$, i.e., the blowup rate is slightly faster than a square root in agreement with the theoretical predication (81).⁹

5.3.2. Collapsing ψ_{S_m} solutions

We solve the supercritical NLS with $\sigma = 1.1$ with the initial condition $\psi_0 = \psi_{S_m}(t = 0)$, where $f_c = 0.43$ and $s(0) = 4.079 \times 10^{-4}$. If the solution is stable, then it should undergo an equal-rate collapse at a square-root blowup rate. To see whether this is the case, we calculate $r_{\max}(t)$, see Eq. (85), and plot it as a function of L . Fig. 28(A) shows that the best-fitting α for $r_{\max} \approx r_0 L^\alpha$ is $\alpha = 0.823$. Also, we plot the blowup rate L as a function of $T_c - t$, in Fig. 28(B), and find that the best-fitting exponent p for $L \sim f_c(T_c - t)^p$ is $p \approx 0.547$. Therefore, we observe that the solution neither undergoes equal-rate collapse nor does it collapse at a square-root blowup rate. The measured values of α and p , however, are in perfect fit with those of the ψ_{Q_m} profile. Indeed, the measured value of $\alpha = 0.823$ differs from the predicted value of α , see Eq. (80), by about 0.6% and the measured blowup rate $p = 0.547$ differs from the predicted blowup rate, see Eq. (81), by about 0.55%.

These results suggest that ψ_{Q_m} is a strong attractor for radially-symmetric vortex solutions of the supercritical NLS, while ψ_{S_m} is unstable. Note that this is also the case in the critical NLS, where ψ_{G_m} is stable, while ψ_{R_m} is unstable, see Section 4.6.

6. Numerical methods

The numerical methods used in this study are the same as in [8]. The notable differences, due to the vorticity, are as follows.

(1) Solution of the NLS (2) with a radially-symmetric vortex initial condition:

- (a) In this case, we actually solve Eq. (9).

⁹ In the cases $\sigma = 1.8$ and $\sigma = 1.9$, the value of L recovered from the simulations turned out to be somewhat noisy. While we were able to extract the value of α from $r_{\max} \approx r_0 L^\alpha$, we were unable to reliably extract the blowup rate, a task which involves differentiation of L . We note that in the simulations of supercritical rings in the vortex-free case, the value of L also turned out noisier for $\sigma = 1.8$ and $\sigma = 1.9$, but the noise was on a smaller scale which enabled the extraction of the blowup rate. Therefore, in that case ([11, Figure 24]) we were able to observe the jump discontinuity in the blowup rate at $\sigma = 2$, predicted in (81).

- (b) Simulations of collapsing vortex solutions are more demanding than in the vortex-free case. The reason is that vortex solutions vanish at the origin, hence as they collapse the amplitude difference between the origin and the ring peak becomes larger and larger, contributing to huge gradients in the solution. In contrast, the value of non-vortex rings at the origin increases at the same rate as the maximal ring amplitude increases as it collapses. Hence, the amplitude difference between the origin and the ring peak remains constant during the collapse and is typically “only” two orders of magnitude.
 - (c) We use the iterative grid redistribution (IGR) method [31]. In the vortex-free case, we used the weight function $w = \sqrt{1 + |A_r|^2 + |A_{rr}|}$. However, since for vortices $|A| \sim r^m$ around $r = 0$, the value of w near the origin is small, leading to subresolution around the origin where exceedingly high gradients develop, see (b). To ensure that grid points are also attracted towards the origin, we choose $w = \sqrt{1 + |\nabla\psi|^2 + |\psi_{rr}|}$ where $|\nabla\psi|^2 = |A_r|^2 + \frac{m^2}{r^2}|A|^2$ and $|\psi_{rr}| = |A_{rr}|$.
 - (d) The boundary condition at $r = 0$ is $A(r = 0) = 0, A_r(0) = 0$.
- (2) **Solution of Eq. (29) for G_m and Eq. (77) for S_m :** Since $G(r) = r^m g(r)$ around $r = 0$, see Lemma 7, to solve Eq. (29) for a given g_0 and f_c , we first solve Eq. (31) for $g_m = G_m/r^m$ in the region $[0, 1]$ with the initial condition $g_m(0) = g_0$. Then, we use this solution to solve Eq. (29) in the region $(1, \infty)$ with the initial conditions $G_m(1) = g_m(1)$ and $G'_m(1) = m g_m(1) + g'_m(1)$. The same method is used for the calculation of the solution of Eq. (77) for S_m . In order to find the relation between g_0 and f_c , we use the same method as in [8] for G_m , and [32, Algorithm 1] for S_m .

Acknowledgments

We thank Steven Schochet for useful discussions. This research was partially supported by Grant No. 2006-262 from the United States–Israel Binational Science Foundation (BSF), Jerusalem, Israel. The research of Nir Gavish was also partially supported by the Israel Ministry of Science Culture and Sports.

Appendix A. Proof of Lemma 2

Item 1 is immediate. To prove item 2, let us use a cylindrical coordinate system $(\hat{e}_r, \hat{e}_\theta)$. Then, for $\psi = A(t, r)e^{im\theta}$, see Lemma 1, $\|\nabla\psi\|_2^2 = \|\psi_r \hat{e}_r + \psi_\theta \frac{\hat{e}_\theta}{r}\|_2^2 = \|\psi_r\|_2^2 + \|\frac{1}{r}\psi_\theta\|_2^2 = \|A_r\|_2^2 + m^2 \|\frac{A}{r}\|_2^2$. Items 3–5 follow directly from item 2. To prove item 6, we note that

$$M(t) = \int r \hat{e}_r \times \text{Im}(\psi^* \nabla \psi) \, dx = \int r \hat{e}_r \times \text{Im} \left(\psi^* \left(\psi_r \hat{e}_r + \frac{1}{r} \psi_\theta \hat{e}_\theta \right) \right) \, dx = \int \text{Im}(\psi^* \psi_\theta) \, dx.$$

Therefore, for $\psi = A(t, r)e^{im\theta}$, $M(t) = m \|A\|_2^2 = mP(A) = mP(\psi)$.

Appendix B. Proof of Lemma 3

Let us look for a solution of (13) of the form $R_m = r^\ell q_m(r)$ where $q_m(0) \neq 0$ and $q'_m(0) = 0$. Substituting this form into Eq. (13) gives

$$q''_m(r) + \frac{2\ell + 1}{r} q'_m - q_m + \frac{\ell^2 - m^2}{r^2} q_m + r^{2\sigma\ell} q_m^{2\sigma+1} = 0. \tag{B.1}$$

Eq. (B.1) has a regular singular point at $r = 0$, hence there exist solutions of the form $q_m(r) = r^\alpha \sum_{i=0}^\infty a_i r^i$, where α is solution of the indicial equation $\alpha^2 + 2\ell\alpha + \ell^2 - m^2 = 0$. Since $q_m(0) \neq 0$, $\alpha = 0$ and therefore $\ell_{1,2} = \pm m$. Since $q_m(0) \neq 0$, the term $r^{2\sigma\ell} q_m^{2\sigma+1}$ is regular at $r = 0$ only if $\ell > 0$, hence $\ell = m$. Substituting $\ell = m$ into (B.1) gives (15).

Appendix C. Proof of Lemma 6

From the proof of Lemma 13 it follows that $J_m[R_{m,k}] = \frac{1}{2} \|R_{m,k}\|_2^2$, for any solution $R_{m,k}$ of (18), and that the minimum of J_m is obtained by $R_{m,k}$ for some k . Hence, the ground state of (18) is the minimizer of $J_m[f]$. From the proof of Lemma 12, the minimizer of $J_m[f]$ is positive. Since $R_{m,0}$ is a unique positive solution of (18), it follows that the ground state of (18) is $R_{m,0}$.

Appendix D. Proof of Lemma 12

Following Weinstein [21], from the definition of infimum, there exists a sequence $u_n \in \mathcal{F}$ such that $J_m[u_n] \rightarrow \alpha > 0$. Since $J_m[u_n] = J_m[|u_n|]$ for $u_n \in \mathcal{F}$, we can take $u_n \geq 0$. Let $u_n^{\lambda,\mu}(r) = \mu u_n(\lambda r)$. It is easy to see that $J_m[u_n^{\lambda,\mu}] = J_m[u_n]$. Therefore,

we can choose λ_n and μ_n such that $J_m[u_n^{\lambda,\mu}] = J_m[u_n]$ and $\|u_n^{\lambda,\mu}\|_2 = \|\nabla u_n^{\lambda,\mu}\|_2 = 1$. Therefore, we obtain a sequence $u_n = u_n^{\lambda,\mu}$ with the following properties:

$$u_n = u_n(r) \geq 0, \quad u_n \in \mathcal{F},$$

$$\|u_n\|_2 = \|\nabla u_n\|_2 = 1, \quad J_m[u_n] = \frac{1}{\|u_n\|_4^4} \left[1 + \left\| \frac{u_n}{r} \right\|_2^2 \right] \longrightarrow \inf_{f \in \mathcal{F}} J[f].$$

Since u_n is bounded in H^1 , it has a subsequence such that $u_n \rightharpoonup u$ weakly in H^1 . Therefore, u_n and ∇u_n converge weakly in L^2 to u and ∇u , respectively. It thus follows that $\|u\|_2 \leq 1$ and $\|\nabla u\|_2 \leq 1$. The Compactness Lemma, see [21], then ensures strong convergence of $u_n \rightarrow u$ in L^4 , i.e.,

$$\frac{1}{\|u\|_4^4} = \lim_{n \rightarrow \infty} \frac{1}{\|u_n\|_4^4}. \tag{D.1}$$

Since u_n/r is bounded in L^2 , it has a subsequence such that $u_n/r \rightharpoonup v$ weakly in L^2 . We now prove that $v = u/r$. Indeed, for any test function $\varphi \in \tilde{\mathcal{F}}$, where $\tilde{\mathcal{F}} = \left\{ f \mid f, \frac{f}{r} \in L^2 \right\}$, $\int \frac{u_n}{r} \varphi = \int u_n \frac{\varphi}{r}$. Hence, $\int v \varphi = \lim_{n \rightarrow \infty} \int \frac{u_n}{r} \varphi = \lim_{n \rightarrow \infty} \int u_n \frac{\varphi}{r} = \int u \frac{\varphi}{r}$.

Since $\tilde{\mathcal{F}}$ is dense in L^2 , it follows that for any test function $\varphi \in L^2$, $\int v \varphi = \int \frac{u}{r} \varphi$.

Hence, $v = u/r$ and $u_n/r \rightharpoonup u/r$. The weak convergence of u_n/r to u/r in L^2 implies that

$$\left\| \frac{u}{r} \right\|_2 \leq \liminf_{n \rightarrow \infty} \left\| \frac{u_n}{r} \right\|_2. \tag{D.2}$$

By (D.1) and (D.2), $J[u] \leq \lim_{n \rightarrow \infty} \inf J[u_n]$. Since $\lim_{n \rightarrow \infty} J[u_n]$ exists and is equal to $\inf_{f \in \mathcal{F}} J[f]$,

$$J[u] \leq \lim_{n \rightarrow \infty} \inf J[u_n] = \inf_{f \in \mathcal{F}} J[f].$$

Therefore, $J[u] = \inf_{f \in \mathcal{F}} J[f]$.

Appendix E. Proof of Lemma 13

We generalize Weinstein’s calculation of the critical power for $m = 0$ [21] to ring vortices ($m \neq 0$). By Lemma 12, there exists a minimizer of the functional $J_m[f]$. We first show that, up to multiplication by a constant phase factor, the minimizer of $J_m[f]$ is real-valued:

Lemma 30. *Let $J_m[f]$ be given by (35), and let $h(r) = A(r)e^{ig(r)}$ be a minimizer of $J_m[h]$ where A and g are real. Then, $g \equiv \text{Const}$.*

Proof. Since, $J_m[h] = J_m[A] + \frac{\|g'\|_2^2 \|A\|_2^2}{\|A\|_4^4}$, then $J_m[A] \leq J_m[h]$ if and only if $g \equiv \text{const}$ and $J_m[A] = J_m[h]$. \square

Lemma 31. *Let $J_m[f]$ be given by (35). Then the minimum is obtained for $f = \mu R_{m,0}(\lambda r)$ where $R_{m,0}$ is the ground state solution of Eq. (18) and, $\lambda > 0$ and $\mu \in \mathbb{R}$. Furthermore, $\min_{f \in \mathcal{F}} J_m[f] = \frac{1}{2} \|R_{m,0}\|_2^2$.*

Proof. Let f be a minimizer of J_m . Then f satisfies the Euler–Lagrange equation

$$\left. \frac{dJ_m[f + \varepsilon g]}{d\varepsilon} \right|_{\varepsilon=0} = 0, \quad \forall g \in \mathcal{F}. \tag{E.1}$$

Dropping the tilde sign and carrying out the variational derivative gives

$$\left[2 \frac{\|f\|_2^2}{\|f\|_4^4} \int \nabla f \nabla g \, dx + 2 \frac{\|\nabla f\|_2^2}{\|f\|_4^4} \int f g \, dx - 4 \frac{\|f\|_2^2 \|\nabla f\|_2^2}{\|f\|_4^8} \int f^3 g \, dx \right]$$

$$+ m^2 \left[2 \frac{\|f\|_2^2}{\|f\|_4^4} \int \frac{f g}{r^2} \, dx + 2 \frac{\|f/r\|_2^2}{\|f\|_4^4} \int f g \, dx - 4 \frac{\|f/r\|_2^2 \|f\|_2^2}{\|f\|_4^8} \int f^3 g \, dx \right] = 0.$$

Multiplying by $\|f\|_4^4/2\|f\|_2^2$ and reorganizing the last equation, we obtain

$$\int \nabla f \nabla g \, dx + \frac{\|\nabla f\|_2^2 + m^2 \|f/r\|_2^2}{\|f\|_2^2} \int f g \, dx - 2 \frac{\|\nabla f\|_2^2 + m^2 \|f/r\|_2^2}{\|f\|_4^4} \int f^3 g \, dx + m^2 \int \frac{f g}{r^2} \, dx = 0.$$

Integrating by parts gives,

$$\int g \left[-\Delta f + \left(w_f + \frac{m^2}{r^2} \right) f - \beta_f f^3 \right] \mathbf{d}\mathbf{x} = 0, \tag{E.2}$$

where $w_f = \frac{\|f'\|_2^2 + m^2 \|f/r\|_2^2}{\|f\|_2^2}$ and $\beta_f = 2 \frac{\|f'\|_2^2 + m^2 \|f/r\|_2^2}{\|f\|_4^4}$.

Let $f^{\lambda, \mu}(r) = \mu f(\lambda r)$. It is easy to see that $J_m[f^{\lambda, \mu}] = J_m[f]$. Therefore, we can eliminate w_f and β_f from (E.2) by setting

$$\lambda_0 = \sqrt{w_f}, \quad \mu_0 = \sqrt{\frac{w_f}{\beta_f}}, \tag{E.3}$$

so that Eq. (E.2) becomes

$$\int g \left[-\Delta f^{\lambda_0, \mu_0} + \left(1 + \frac{m^2}{r^2} \right) f^{\lambda_0, \mu_0} - (f^{\lambda_0, \mu_0})^3 \right] \mathbf{d}\mathbf{x} = 0. \tag{E.4}$$

Let us denote

$$R_m = f^{\lambda_0, \mu_0}. \tag{E.5}$$

Since (E.4) is valid for all $g \in \mathcal{F}$, we have that $R_m(r)$, the minimizer of J_m , is a solution of (18). Furthermore, from (E.2), (E.3) and (E.5)

$$\|R_m\|_2^2 = \|f^{\lambda_0, \mu_0}\|_2^2 = \frac{\mu_0^2}{\lambda_0^2} \|f\|_2^2 = 2 \frac{\|f'\|_2^2 + m^2 \|f/r\|_2^2}{\|f\|_4^4} \|f\|_2^2 = 2J_m[f] = 2J_m[f^{\lambda_0, \mu_0}] = 2J[R_m],$$

giving

$$J_m[R_m] = \min_{f \in \mathcal{F}} J_m[f] = \frac{1}{2} \|R_{m,0}\|_2^2. \tag{E.6}$$

The optimal constant C_m is given by $C_m = \frac{1}{\min_{f \in \mathcal{F}} J_m[f]}$. Hence, by (E.6), $C_m = \frac{1}{J_m[R_m]} = \frac{2}{\|R_{m,0}\|_2^2}$. \square

Appendix F. Proof of Lemma 18

Let $\psi_0 = A_0 e^{im\theta}$. When (54) holds, the center of mass $\bar{\mathbf{x}}$ is at $(x, y) = 0$, $\bar{\mathbf{x}} = \int \mathbf{x} A_0^2 \mathbf{d}x \mathbf{d}y = 0$. The change in the center of mass is constant and is given by the linear momentum (see, e.g., [1]), i.e., $\frac{d\bar{\mathbf{x}}}{dt} \equiv \frac{1}{2\|\psi_0\|_2^2} \int \text{Im}(\psi_0 \nabla \psi_0^*)$. Let us use a cylindrical coordinate system $(\hat{e}_r, \hat{e}_\theta)$. Then,

$$\begin{aligned} \int \text{Im}(\psi_0 \nabla \psi_0^*) r \mathbf{d}r \mathbf{d}\theta &= \int \text{Im} \left(\psi_0 \left(\psi_r \hat{e}_r + \frac{1}{r} \psi_\theta \hat{e}_\theta \right)^* \right) r \mathbf{d}r \mathbf{d}\theta \\ &= \int \text{Im} \left[\frac{1}{2} (A_0^2)_r \hat{e}_r + \left(i \frac{mA^2}{r} + \frac{1}{2r} (A_0^2)_\theta \right) \hat{e}_\theta \right] r \mathbf{d}r \mathbf{d}\theta = m \int A_0^2 \hat{e}_\theta \mathbf{d}r \mathbf{d}\theta = 0, \end{aligned}$$

where in the last stage we substituted $\hat{e}_\theta = (-\sin \theta, \cos \theta)$ and used (54).

Appendix G. Derivation of Eq. (67)

Substitution of (66) into the NLS gives, for $\mathcal{O}(\mu)$

$$\begin{aligned} &\underbrace{i \frac{d}{dt} \psi_{G_{m,0}}(t, r, \theta) + \Delta \psi_{G_{m,0}} + |\psi_{G_{m,0}}|^2 \psi_{G_{m,0}}}_{=0} \\ &+ \mu \cos(\Omega t) e^{\delta \Omega \tau} \left[\underbrace{i \frac{d}{dt} \psi_{G_{m,0}} + \Delta \psi_{G_{m,0}} + |\psi_{G_{m,0}}|^2 \psi_{G_{m,0}}}_{=0} + i \frac{\delta \Omega}{L^2(t)} \psi_{G_{m,0}} - \frac{\Omega^2}{L^2(t) \rho^2} \psi_{G_{m,0}} \right] \\ &+ 2\mu_r \cos(\Omega t) e^{\delta \Omega \tau} |\psi_{G_{m,0}}|^2 \psi_{G_{m,0}} = 0. \end{aligned}$$

Hence, $(\mu_r + i\mu_i) \left(i\delta \Omega - \frac{\Omega^2}{\rho^2} \right) + 2\mu_r L^2(t) |\psi_{G_{m,0}}|^2 = 0$.

Since $|\psi_{G_{m,0}}| = \frac{1}{L}G_{m,0}(\rho)$, the equation for the real and imaginary parts can be written as $B \begin{pmatrix} \mu_r \\ \mu_i \end{pmatrix} = 0$, where $B = \begin{pmatrix} 2G_{m,0}^2(\rho) - \left(\frac{\Omega}{\rho}\right)^2 & -\delta_{\Omega} \\ \delta_{\Omega} & -\left(\frac{\Omega}{\rho}\right)^2 \end{pmatrix}$.

A non-trivial solution exists if $|B| = 0$, from which follows Eq. (67) for δ_{Ω} .

Appendix H. Proof of Theorem 23

Define

$$B_k(r, \theta) = S(\psi)(t_k, r, \theta) = L(t_k)e^{i\gamma(t_k)}\psi(t_k, L(t_k)r, \theta) \quad (\text{H.1})$$

where L is given by (58). Then, $\|B_k\|_2 \equiv \|\psi_0\|_2$ and $\|\nabla B_k\|_2 = L(t_k)\|\nabla\psi(t_k, \cdot)\|_2 \equiv 1$.

Since B_k is bounded in H^1 , it has a subsequence such that $B_k \rightharpoonup \Psi$ weakly in H^1 . Therefore, B_k and ∇B_k converge weakly in L^2 to Ψ and $\nabla\Psi$, respectively. Hence,

$$\|\Psi\|_2 \leq \liminf_{k \rightarrow \infty} \|B_k\|_2, \quad \|\nabla\Psi\|_2^2 \leq \liminf_{k \rightarrow \infty} \|\nabla B_k\|_2^2. \quad (\text{H.2})$$

By Lemma 1, $\psi(t, r, \theta) = A(t, r)e^{im\theta}$. Hence $B_k(r, \theta) = L(t_k)e^{i\gamma(t_k)}A(t_k, L(t_k)r)e^{im\theta}$.

Let $b_k = B_k e^{-im\theta}$, then $b_k(r) = L(t_k)e^{i\gamma(t_k)}A(t_k, L(t_k)r)$. By Lemma 2, $A \in H_{\text{radial}}^1$. In addition,

$$\|b_k\|_2 = \|\psi_0\|_2, \quad \|\nabla b_k\|_2 = L(t_k)\|\nabla A(t_k, \cdot)\|_2 = \frac{\|\nabla A(t_k, \cdot)\|_2}{\|\nabla\psi\|_2} = \frac{\|A_r\|_2}{\|A_r\|_2 + m^2\|A/r\|_2^2} \leq 1.$$

Since b_k is bounded in H_{radial}^1 , the Compactness Lemma for radial functions, see [21], ensures strong convergence of b_k to $\Psi e^{-im\theta}$, hence of B_k to Ψ , in L^p for $2 < p < \infty$. In particular, $\|\Psi\|_4 = \lim_{k \rightarrow \infty} \|B_k\|_4$. From the last relation and (H.2) it follows that

$$H(\Psi) \leq \liminf_{k \rightarrow \infty} H(B_k) \leq \liminf_{k \rightarrow \infty} L^2(t_k)H(\psi_0) = 0.$$

Therefore, from Lemma 13 it follows that $\|\Psi\|_2^2 \geq P_{\text{cr}}(m)$.

Appendix I. Proof of Theorem 24

For any $\varepsilon > 0$, $\|\phi_k\|_{L^2(r < \varepsilon/L(t_k))} = \|\psi(t_k)\|_{L^2(r < \varepsilon)}$, where ϕ_k is defined by (H.1). Therefore, for any $R > 0$, if k is sufficiently large, $\|\phi_k\|_{L^2(r < R)} \leq \|\psi(t_k)\|_{L^2(r < \varepsilon)}$.

Since ϕ_k converges weakly to Ψ in L^2 , see the proof of Theorem 23, it also converges weakly to Ψ in $L^2(r < R)$, hence $\|\Psi\|_{L^2(r < R)} \leq \lim_{j \rightarrow \infty} \inf \|\phi_k\|_{L^2(r < R)}$.

Therefore, $\|\Psi\|_{L^2(r < R)} \leq \lim_{j \rightarrow \infty} \inf \|\psi(t_k)\|_{L^2(r < \varepsilon)}$. Since this holds for all R , we have from Theorem 23, $P_{\text{cr}}(m) \leq \|\Psi\|_{L^2}^2 \leq \lim_{j \rightarrow \infty} \inf \|\psi(t_k)\|_{L^2(r < \varepsilon)}^2$, which proves Theorem 24.

References

- [1] C. Sulem, P. Sulem, The Nonlinear Schrödinger Equation, Springer, New-York, 1999.
- [2] A.S. Desyatnikov, L. Torner, Y.S. Kivshar, in: E. Wolf (Ed.), Optical Vortices and Vortex Solitons, in: Progress In Optics, vol. 47, 2005, pp. 219–319.
- [3] V. Kruglov, Y. Logvin, V. Volkov, The theory of spiral laser beams in nonlinear media, J. Modern Opt. 39 (1992) 2277–2291.
- [4] V. Kruglov, V. Volkov, R. Vlasov, V. Drits, Auto-waveguide propagation and the collapse of spiral light beams in non-linear media, J. Phys. A: Math. Gen. 21 (1988) 4381–4395.
- [5] L. Vuong, T. Grow, A. Ishaaya, A. Gaeta, G. Hooft, E. Eliel, G. Fibich, Collapse of optical vortices, Phys. Rev. Lett. 96 (2006) 133901.
- [6] G. Fibich, B. Ilan, Self focusing of elliptic beams: An example of the failure of the aberrationless approximation, JOSA B 17 (2000) 1749–1758.
- [7] F. Merle, P. Raphael, Sharp upper bound on the blow-up rate for the critical nonlinear Schrödinger equation, Geom. Funct. Anal. 13 (2003) 591–642.
- [8] G. Fibich, N. Gavish, X. Wang, New singular solutions of the nonlinear Schrödinger equation, Physica D 211 (2005) 193–220.
- [9] J. Soto-Crespo, D. Heatley, E. Wright, N. Akhmediev, Stability of the higher-bound states in a saturable self-focusing medium, Phys. Rev. A 44 (1991) 636–644.
- [10] J. Soto-Crespo, E. Wright, N. Akhmediev, Recurrence and azimuthal-symmetry breaking of a cylindrical Gaussian beam in a saturable self-focusing medium, Phys. Rev. A 45 (1992) 3168–3174.
- [11] G. Fibich, N. Gavish, X. Wang, Singular ring solutions of critical and supercritical nonlinear Schrödinger equations, Physica D 231 (2007) 55–86.
- [12] C.J. Budd, Asymptotics of multibump blow-up self-similar solutions of the nonlinear Schrödinger equation, SIAM J. Appl. Math. 62 (2001) 801–830.
- [13] S. Vlasov, V. Petrishchev, V. Talanov, Averaged description of wave beams in linear and nonlinear media, Izv. Vuz Radiofiz 14 (1971) 1353–1363 (in Russian); Radiophys. Quantum Electron. 14 (1971) 1062–1070 (in English).
- [14] J. Iaiia, H. Warchall, Nonradial solutions of semilinear elliptic equation in two dimensions, J. Differential Equations 119 (1995) 533–558.
- [15] T. Mizumachi, Vortex solitons for 2d focusing nonlinear Schrödinger equation, Differential Integral Equations 18 (4) (2004) 431–450.

- [16] T. Mizumachi, Instability of bound states for 2d nonlinear Schrödinger equations, *Discrete Contin. Dyn. Syst.* 13 (2) (2005) 413–428.
- [17] T. Mizumachi, Instability of vortex solitons for 2d focusing NLS, *Adv. Differential Equations* 12 (3) (2007) 241–264.
- [18] L.D. Menza, Numerical computation of solitons for optical systems, PrePrint.
- [19] V. Talanov, Focusing of light in cubic media, *JETP Lett.* 11 (1970) 199–201.
- [20] R. Johnson, X. Pan, On an elliptic equation related to the blow-up phenomenon in the nonlinear Schrödinger equation, *Proc. Roy. Soc. Edinburgh Sect. A* 123 (1993) 763–782.
- [21] M. Weinstein, Nonlinear Schrödinger equations and sharp interpolation estimates, *Comm. Math. Phys.* 87 (1983) 567–576.
- [22] F. Merle, On uniqueness and continuation properties after blow-up time of self-similar solutions of nonlinear Schrödinger equation with critical exponent and critical mass, *Commun. Pure Appl. Math.* 45 (1992) 203–254.
- [23] F. Merle, Determination of blow-up solutions with minimal mass for nonlinear Schrödinger equation with critical power, *Duke Math. J.* 69 (1993) 427–454.
- [24] G. Fibich, A. Gaeta, Critical power for self-focusing in bulk media and in hollow waveguides, *Optim. Lett.* 25 (2000) 335–337.
- [25] F. Merle, Nonexistence of minimal blow-up solutions of equations $iu_t = -\Delta u - k(x)|u|^{4/N}u$ in \mathbf{R}^N , *Ann. Inst. H. Poincaré Phys. Théor.* 64 (1996) 33–85.
- [26] G. Fibich, F. Merle, Self-focusing on bounded domains, *Physica D* 155 (2001) 132–158.
- [27] M. Weinstein, The nonlinear Schrödinger equation — singularity formation, stability and dispersion, *Contemp. Math.* 99 (1989) 213–232.
- [28] F. Merle, Y. Tsutsumi, L^2 concentration of blow-up solutions for the nonlinear Schrödinger equation with critical power nonlinearity, *J. Differential Equations* 84 (1990) 205–214.
- [29] A. Vincotte, L. Berge, Atmospheric propagation of gradient-shaped and spinning femtosecond light pulses, *Physica D* 223 (2006) 163–173.
- [30] P. Raphael, Existence and stability of a solution blowing up on a sphere for a L^2 supercritical non linear Schrödinger equation, *Duke Math. J.* 134 (2) (2006) 199–258.
- [31] W. Ren, X. Wang, An iterative grid redistribution method for singular problems in multiple dimensions, *J. Comput. Phys.* 159 (2000) 246–273.
- [32] C.J. Budd, S. Chen, R.D. Russell, New self-similar solutions of the nonlinear Schrödinger equation with moving mesh computations, *J. Comput. Phys.* 152 (1999) 756.